

# An Infrared Search for Star-Forming Galaxies at $z > 2$

H. Teplitz<sup>1</sup>, M. Malkan, I.S. McLean

Department of Physics & Astronomy, Division of Astronomy

University of California at Los Angeles

Los Angeles, CA 90095-1562

hit@binary.gsfc.nasa.gov, malkan@astro.ucla.edu, mclean@astro.ucla.edu

## ABSTRACT

We report the cumulative results of an on-going near-infrared search for redshifted H $\alpha$  emission from normal galaxies at  $z > 2$ . An infrared search reduces the bias due to reddening. Using narrow-band imaging with the Near Infrared Camera on the Keck I 10-m telescope, a survey area of almost 12 square arcminutes has been covered. Target regions were selected by matching the redshifts of QSO emission and metal-line absorptions to our available filters. The survey depth is  $7 \times 10^{-17}$  ergs/cm<sup>2</sup>/s ( $3\sigma$ ) in H $\alpha$  and  $K' \simeq 22$ . Eleven H $\alpha$ -emitters, plus two Seyfert I objects, have been discovered. The high density of galaxy detections, corresponding to a co-moving volume density of  $0.0135 + 0.0055 - 0.0035$  Mpc<sup>-3</sup>, makes it unlikely that all of the H $\alpha$  flux in these objects is the result of active nuclei. There is a strong suggestion of clustering in the environments of metal-line absorbers. Each candidate galaxy lies typically within a projected distance of 250kpc of the QSO line of sight and is resolved but compact. The average Star Formation Rate inferred for the galaxies from the H $\alpha$  flux is 50 M $_{\odot}$ /yr, significantly higher than current day star-forming galaxies, but consistent with other estimates for galaxies at high redshift.

*Subject headings:* galaxies : individual — galaxies : evolution — cosmology : observation — infrared : galaxies

## 1. Introduction

In Malkan, Teplitz, & McLean 1995 (hereafter MTM95), we presented one of the first detections of a star-forming galaxy at  $z > 2$  and strong evidence that it belongs to a group

---

<sup>1</sup>now an NOAO Research Associate at Goddard Space Flight Center, Code 681, GSFC, Greenbelt, MD 20771

of such objects (Malkan, Teplitz, & McLean 1996, hereafter MTM96). The two years since then have seen a dramatic increase in the normal galaxies known at high redshift; that is, galaxies that are not obviously powered by a dominant non-stellar source, such as a Seyfert nucleus. Steidel *et al.* (1996) have discovered galaxies at  $z > 3$  by observing the drop off in the UV continuum below the Lyman limit. Other groups (*e.g.* Francis *et al.* 1996, Pascarelle *et al.* 1996) have found Ly $\alpha$  emission from galaxies at  $z > 2$ . Yee *et al.* (1996) and Trager *et al.* (1996) have serendipitously found gravitationally lensed galaxies at  $z > 2.5$ . All of these other discoveries relied on the rest-frame UV, where the effects of intrinsic reddening are largest. In this paper, we present the results of an ongoing near-IR search for redshifted H $\alpha$  emission from normal galaxies at  $z > 2$ ; at a redshift of  $z=2.05$ , H $\alpha$  moves into the K-band at  $2.0 \mu\text{m}$ . By finding line emission from the rest-frame optical, we obtain a sample which is potentially more complete because it avoids most of the bias against reddened galaxies. Further, H $\alpha$  is directly related to the on-going formation of the youngest, most massive stars (Kennicutt, 1983).

Using 1% wide ( $\Delta\lambda/\lambda$ ) interference filters, we can detect line emission by comparing the flux in the narrow-band to the continuum measured in a standard broad-band  $2 \mu\text{m}$  filter, such as K' (1.95-2.30  $\mu\text{m}$ ). Objects which have no line emission will all have the same narrow-to-broad band color, as determined by the relative widths and transmissions of the two filters. An object which has H $\alpha$  emission at the right redshift however, will be relatively brighter in the narrow filter. In our typical exposure times, we detect objects at  $K' \simeq 22$  ( $3\sigma$ ) with an H $\alpha$  flux  $\geq 7 \times 10^{-17} \text{ergs/cm}^2/\text{s}$  (corresponding to  $\gtrsim 30 M_{\odot}/\text{yr}$ ) at the 99.5% confidence level. To increase our chance of finding new galaxies in the redshift window given by one of our narrow-band filters, we survey fields containing known objects (QSOs or metal absorption-line systems) at redshifts which place H $\alpha$  in the centers of those filter bandpasses. Follow-up optical spectroscopy and photometry is obtained of fields containing a detection.

This infrared survey has revealed 5 strong H $\alpha$ -emitters, 6 weaker ones, 2 Seyfert Is, and several objects with very red colors but no apparent line emission. The first object detected (MTM95) appears to belong to a cluster of galaxies at  $z=2.5$  (MTM96). We present here details of the survey to date. First we will discuss the individual fields, and then the conclusions we draw from the sample as a whole. Throughout this paper, we assume  $H_0 = 50 \text{ km s}^{-1}\text{Mpc}^{-1}$  and  $q_0 = 0.5$ .

## 2. Observations

All observations in this survey were taken at the 10-m Keck I and II telescopes. We obtained images of 23 fields with the Near IR Camera (NIRC), which has a  $256 \times 256$  pixel InSb array, (Matthews *et al.*, 1994) and a field of view of  $38'' \times 38''$ ;  $0.15''/\text{pixel}$ . Although the field of view is small, this instrument has high throughput and excellent depth under good seeing conditions. Deep B,V and I imaging of the same fields was obtained with the Low Resolution Imaging Spectrometer (LRIS), which has a  $2048 \times 2048$  pixel CCD detector, with a field of view of  $5'$  by  $7'$  (Oke *et al.*, 1995).

The Near IR Camera has five narrow-band filters in the 2–2.5  $\mu\text{m}$  range. For the broad-band, we use the  $K'$  filter (Wainscoat & Cowie 1992). Table 1 lists the properties of each narrow-band filter, including their transmission as measured from our extensive photometry of object fields and calibration stars. The molecular hydrogen transition filters have significantly lower transmission than the other three, so we soon decided not to use them. The filter centered at 2.24  $\mu\text{m}$ , called the “K-continuum” filter, is wider than the others, with  $\Delta\lambda/\lambda = 2.2\%$ . The wider band pass makes this filter less attractive, since it increases the sky background without any increase in emission-line flux. However, the tradeoff between contrast and search volume was favorable for a number of fields on our target list that included multiple absorption line systems within the redshift range probed by that filter ( $z=2.42\text{--}2.46$ ), and in those cases we opted to use it.

All IR observations were taken using the “dither pattern” technique, in which many small displacements (*e.g.*  $3\text{--}5''$ ) of the telescope are made between successive exposures on the same field (see McLean & Teplitz, 1996, among many others), and twilight flat-fields were used to divide out variations in detector response. Observations were reduced as follows. Each frame was divided by the flat-field, and then an individual sky frame was created for each exposure from a running median of the other object frames taken nearest in time to each observation. This specific sky frame was then subtracted from the object frame. In cases where a flat field was unavailable, the sky frames were generated first, then normalized to their mode and used as a flat, while sky subtraction was handled in aperture photometry. Detailed comparisons showed little appreciable loss in the signal-to-noise ratio when using the latter method. All data reduction was performed using IRAF routines. A similar technique was used for I-band observations. The B and V band CCD observations, however, were taken without dithering, and they were divided by twilight flats. Objects were identified with the SExtractor program for galaxy identification and analysis (Bertin & Arnouts, 1996) and the object list was checked by eye for each frame.

Photometry was performed in circular apertures of 10 pixels ( $1.5''$ ) diameter (approximately 2.5 times the seeing disk), which corresponds to 12 kpc at  $z=2.5$ . The size

of the aperture was chosen primarily to obtain optimal signal to noise (see Thompson *et al.*, 1995, and Howell 1989). The mode of the pixels in a “sky annulus” around the aperture was subtracted, to ensure proper sky subtraction in addition to that performed in the initial reduction. The same aperture size was used for both broad-band and narrow-band frames. As a check on these results, we also performed photometry in elliptical apertures determined by Kron’s “first moment” (Kron 1980) routine in the SExtractor software. In that case, the apertures were determined in the broad-band frame and then used with the same size and orientation in the narrow-band frame. The flux ratios for each method agreed to better than 10%.

A third check was performed using gaussian fitting. A two dimensional gaussian profile was fitted to each object in the broad band, to determine the shape and amplitude. The same gaussian was fitted to the narrow-band image with only the amplitude allowed to vary. Figure 1 shows a comparison of this method with the aperture photometry.

### Error Analysis

Since we are looking for apparent excess in the broad-band minus narrow-band color, accurate measurement of the photometric errors is essential. Errors in photometry were calculated from the  $1\sigma$  limiting magnitudes. First, photometry was performed on several hundred randomly selected locations within the frame, using the same standard aperture adopted for objects and the same “sky subtraction” annulus. This set of sky measurements was analyzed to obtain the standard deviation of the flux in the apertures. To demonstrate the validity of this method the following procedure was used. For each frame, we inserted fake objects and measured their photometry in the standard aperture. Several hundred such tests were performed across each image. The deviation in these measurements from the flux inserted agreed to better than 5% with the “blank sky” photometric method of determining  $1\sigma$  errors, as expected; except for the random placement of the apertures, the methods should be identical.

The next step in error analysis is to consider the propagation of individual photometric errors into the derived color value. At first we considered adding the individual fractional photometric errors in quadrature. This basic approach is traditionally derived from the first order term in a Taylor expansion of the function into which errors are being propagated. However, the first order terms are not sufficient in the case where the errors are relatively large compared to the measurements themselves. In our case, the large error regime is important, particularly in cases where an object may be detected more strongly in the narrow band than in the broad band. In order to account for higher order terms, we chose

to model the error analysis. We assumed a gaussian distribution of photometric errors and then generated a data set of 100,000 points based on a known ratio of broad to narrow band flux. We remove objects that are less than  $1\sigma$  (after adding the gaussian error) in the broad-band from the simulated population, as they would be undetectable and would not populate our measured color-magnitude diagrams. Using this simulation, we are able to define confidence intervals by simply counting the simulated measurements (see Figure 2).

We find, as expected, that for the regime where errors are relatively small, the traditional approach is accurate. In the case of objects with flux levels less than 5 times the photometric error, the first order error analysis grossly overestimates the error in the color, due to the vanishing denominator. Even in cases of 5-10  $\sigma$  objects, there can be substantial deviation. We adopt the approach of using our empirically derived confidence intervals in evaluating color-magnitude plots.

The derived confidence intervals can be described to a reasonable approximation in terms of a single noise characteristic,  $\Sigma$ . If the broadband minus narrowband magnitude difference for featureless continuum emitters is given by  $R_0$ , then we find that the shape of the upper confidence interval is well approximated by:

$$R(f_b) = R_0 + 2.5 * \log(10^{1+\Sigma/f_b}) \quad (1)$$

where  $f_b$  is the broad band flux. This empirical formula thus gives a good estimate of how large a magnitude difference is required to be significant at the 99.5% confidence level. In our analysis, we use the slightly more precise upper boundary defined by the Monte Carlo simulations.

## Target Selection and Control Fields

Targets were selected from a search of NASA/IPAC Extragalactic Database (NED). We looked for fields containing QSOs, both radio loud and radio quiet, or absorption line systems, both Damped Ly $\alpha$  Absorption or metal line absorption. Objects south of  $-30^\circ$  were not considered. We then selected fields at redshifts within  $\pm 0.3\%$  of the central redshift of the filters. Table 2 describes the observations by date and filter.

In order to determine the effect of our target selection on the density of detections, we need to obtain control observations. We plan to begin such an experiment by observing targets at  $z > 3$  which have no absorption systems at redshifts to place H $\alpha$  in our narrow-band filters. One preliminary observation of this kind detects no emission-line galaxies in one NIRC field around the QSO 1542+4744 with an integration time of 6480 seconds in the narrow band, during which time we reached a  $3\sigma$  limiting flux of  $6 \times 10^{-17}$

ergs/cm<sup>2</sup>/s (as deep as most of the z=2.5 target fields). A shallow observation of the field around the QSO 0234+013 also detects no emission-line galaxies, down to a limiting flux of  $9 \times 10^{-17}$  ergs/cm<sup>2</sup>/s. Two similar observations were carried out by Pahre & Djorgovski (1995) also with NIRC on Keck targeted to known objects at  $z > 3$ , finding no detections in two NIRC fields, with flux limits of  $3 \times 10^{-17}$  ergs/cm<sup>2</sup>/s.

### 3. Individual Fields

Our survey observations always consist of broad-band K' imaging, along with at least one interference filter. Follow-up observations are still ongoing for many fields. We present the results to date in this section. Table 3 lists the photometry currently available for all the H $\alpha$  -emitting objects, as well as the inferred line fluxes and star formation rates.

The Star Formation Rates (SFRs) for objects were inferred using the result from Kennicutt (1983) relating SFR to H $\alpha$  luminosity, assuming a Salpeter Initial Mass Function with an upper mass cutoff of  $100M_{\odot}$ :

$$\text{SFR}(\text{total}) = \frac{L(\text{H}\alpha)}{1.12 \times 10^{41} \text{ergs s}^{-1}} M_{\odot} \text{yr}^{-1} \quad (2)$$

Individual fields are discussed below.

#### Q0114-089

This QSO at  $z_{em}=3.157$  (Osmer, Porter, & Green, 1994) has a metal-line absorption system at  $z=2.2995$  (Sargent *et al.* 1988). We observed the field through the 2.16  $\mu\text{m}$  filter. Figure 3 shows the image and Figure 4 shows the narrow-minus-broad band colors. There are only six objects total in the field, making the zero-excess color hard to define, but four of the six objects lie close to the line predicted from other observations through the same interference filter (Broad/Narrow  $\sim 24$ ). Two objects show up as having excess flux in the narrow filter. The fainter one (object B) appears to be a probable detection, much like other candidates in the survey. The brighter object (A) is harder to explain; it is too bright (K'=15.4) to be a likely star-forming galaxy at  $z=2.3$ . Comparison with the Planetary Camera snapshot image in the HST archives (see Maoz *et al.* 1993) shows the object to be two magnitudes redder than the the QSO, having V=19.8 and V-K=4.4, compared to the QSO which has V-K=2.3. The snapshot image is distorted due to telescope guidance problems, but in both that image and the K-band image (with poor seeing, FWHM=0.75'')

object A appears unresolved. It is thus most likely that object A is a Seyfert 1 at the redshift of the absorber. Object B lies 19.2'' from the QSO, and has an inferred SFR of 59  $M_{\odot}/\text{yr}$ .

### Q0153+045

The QSO 0153+045 has a CIV absorption system at  $z=2.4243$  (York *et al.*, 1991). We have obtained deep K' imaging of this field as well as narrow-band observations through the 2% wide K-continuum filter. Figure 5 shows the narrow vs. broad band colors. One object stands out as a probable H $\alpha$ -emitter. The  $\Delta m$  of this object lies close to the limit that we can detect at  $3\sigma$ ). We initially observed this field January 1996 using fairly typical integration times (1080 seconds in the broad-band, 4050 seconds in the narrow-band). In November 1996, we returned to the field to confirm the detection by independently repeating the observation. We obtained new integrations which were 50% longer in the broad band and 20% longer in the narrow band than the previous ones. Figure 5 shows the average narrow vs. broad band colors from the two observations. While the objects are fairly faint in the broad-band (necessitating the longer integration on the second visit), excellent agreement was found in the two narrow-band observations. The object was confirmed as a probable H $\alpha$ -emitter.

The object is separated from the QSO by 8'', or 64 kpc (see Fig. 6). The inferred SFR for this object is not remarkably high for our survey, being 42  $M_{\odot}/\text{year}$ . We have also obtained I and J images of this field and some area around it. The faint H $\alpha$ -emitter is one of the redder objects detected in the survey. Its I-K' color of 3.5 is nearly as red as that of MTM095355+545428 (with I-K'=3.8). During a night of poor weather, we attempted V band imaging of the field, but obtained only upper limits, suggesting  $V-K \geq 4$ .

### Q0846+156

The field around this  $z=2.928$  QSO (Hazard *et al.*, 1986) was chosen as a target for the Br $\gamma$  filter due to its CIV absorption system at  $z=2.28$  (York *et al.*, 1991). We find one object that is a possible H $\alpha$ -emitter, though it is barely present in the broad-band image (Figure 7) this object is well detected in the narrow-band suggesting that it is indeed emitting strong H $\alpha$  (see Figure 8). If we accept this object as a detection, it is the faintest high- $z$  object in this survey, with  $K' \sim 22$ . It would have SFR=19 $M_{\odot}/\text{yr}$ . Our planned followup of this object was weathered out, so confirmation is still pending.

### MTM0953+549

The quasar SBS0953+549 ( $z_{em}=2.579$ ) was of special interest as a survey target because its spectrum shows a strong absorption system at  $z_{abs} = 2.50176 \pm 0.00004$ , and weaker systems at 2.49174 and 2.50911 (Levshakov 1992). We obtained narrow-band images, through the  $2.30 \mu\text{m}$  CO(2-0) filter, of three adjacent NIRC fields around this object (see Fig. 9) as well as deep BVI photometry of a more extended area. As we reported in MTM96, comparing the broad and narrow-band fluxes reveals three definite  $\text{H}\alpha$ -emitting objects. The brightest of these was confirmed by spectroscopy to be at  $z=2.498$ , and to show absorption lines consistent with a continuum dominated by young stars. In addition, it showed strong UV emission lines, consistent with star formation, or with ongoing star formation and a small active nuclear component. Since then we have obtained narrow band data on four more adjacent fields, which contain one certain  $\text{H}\alpha$ -emitter (well above the  $3\sigma$  limit) and two probable ones (see Fig. 10). The narrow–broad colors for the entire area surveyed are shown in Fig. 10. The new detections are indicated on Figure 9 as objects D,E and F. They lie  $35.7''$ ,  $24.8''$ , and  $24.4''$  (285.6, 198.4, and 195.2 kpc) from the QSO line of sight. Their inferred SFRs are 56, 36 and  $55M_{\odot}/\text{yr}$ . Objects E and F lie closer to the 99.5% confidence limit, having a weaker emission-line flux than object D, but they fell near the boundary of our NIRC fields, and thus we were able to observe them twice, independently confirming the detection.

### HS1700+6416

This field was also chosen for its multiple absorption systems. The QSO’s spectrum shows Lyman series absorptions that fall in all three of the filters in our survey (Vogel & Reimers, 1995). We chose to first observe the absorption systems at  $z = 2.290, 2.308$  that places  $\text{H}\alpha$  in the  $\text{Br}\gamma$  filter. Fig. 11 shows that two objects have a broad–narrow color consistent with probable  $\text{H}\alpha$  emission. These objects are located within  $21''$  of each other, and  $15''$ - $22''$  of the QSO line of sight (see Fig. 12). The objects have inferred SFRs of 33 and  $35M_{\odot}/\text{yr}$ . We obtained followup J band data in poor seeing conditions in March 1997, in which we detected the two objects. The J- $K'$  colors of 1.7 and  $\sim 3.4$  are also consistent with those of galaxies at large distances.

## PC 2149+0221

PC 2149+0221 is a quasar at  $z = 2.304 \pm 0.005$  (Schneider *et al.*, 1994). We observed the field around the QSO (see Fig. 13) in JHK' and with the 2.16  $\mu\text{m}$  Br $\gamma$  filter. Figure 14 shows that one object clearly stands out as having strong H $\alpha$  emission. The dimensionless Equivalent Width of this line ( $\Delta\lambda/\lambda$ ) is 1.0%. Its magnitude of  $K'=18.15$  leads to an inferred Star Formation Rate of 217  $M_{\odot}$  / year. This is the largest SFR in our sample, and would considerably higher than most other galaxies, even at this redshift. The galaxy is extremely compact, with FWHM = 0.69'' compared to a seeing disk of 0.54''. It lies 15'' from the QSO, which projects to a distance of 119kpc at  $z = 2.3$ . The colors of this galaxy are the bluest of any in our H $\alpha$  sample. Its extremely compact morphology and blue colors suggest that this object has an active nucleus from which we were seeing H $\alpha$  emission, and followup spectroscopy confirmed this conclusion, showing broad lines indicative of a Seyfert 1 nucleus (Malkan *et al.* 1998 in preparation).

## 4. Survey Results

To date we have surveyed more than 11 square arcminutes, with  $3\sigma$  line flux sensitivities  $0.5\text{--}1 \times 10^{-16}$  ergs/cm<sup>2</sup>/sec and broad band sensitivities of  $K' \simeq 22$ . The faintest line-emitting galaxy has  $K'=22.1$ . We have detected a total of 5 strong H $\alpha$ -emitting objects ( $\geq 1 \times 10^{-16}$  ergs/cm<sup>2</sup>/s), 6 weaker ones, and two Seyfert 1 galaxies. Some of these objects are clustered in groups of two or three. Table 4 lists the  $K'$  photometry of each QSO in the fields observed.

Figure 15 shows the SFR vs.  $K'$  magnitude for the H $\alpha$ -emitters excluding those where we believe the dominant flux contribution comes from a Seyfert nucleus. We have plotted MTM095355+545428 with the assumption that a third of its H $\alpha$  emission comes from an active nuclear component. The average inferred SFR of detected galaxies is 52  $M_{\odot}$ /year. This rate is significantly higher than most current day star-forming galaxies. It is also higher than some measured SFR for field galaxies at  $z > 2.5$  from optical surveys (Steidel *et al.* 1996), which find an average (without extinction correction) closer to 10  $M_{\odot}$ / year. It is possible that our higher inferred star-formation rates are typical of high redshift emission-line galaxies and that optical searches systematically underestimate star-formation due to reddening of the UV-continuum. The rest-frame EW(H $\alpha$ ) we are seeing is 40Å or more, comparable to what is seen in modern spirals of type Sc or later. If some high- $z$  galaxies have smaller EW's, then our density estimate would be a lower limit.

We can also examine the angular distribution of the detected objects. Figure 16

compares the number of galaxy detections to the area surveyed as a function of radial distances from the QSO line of sight. If we exclude the 0953+549 detections, we find no significant edge to the possible clusters of line-emitters out to  $40''$ . The fact that there is no density enhancement close to the QSO line of sight indicates that the projected surface density does not change over projected separations from 20 to  $\sim 250$  kpc. 0953+549 is the only field that has been surveyed beyond a radius of  $40''$  from the QSO line of sight. Though we detect objects in the most outlying NIRC frames in that region, all of the line-emitters are within  $40''$  of the targeted QSO. This might be providing a marginal hint of an edge to the cluster of galaxies beyond 250 kpc in this field.

All of the  $z > 2$  objects detected are extremely compact. They typically show  $\text{FWHM} \sim 0.9'' \pm 0.2''$ , compared to a usual seeing disk of  $0.6''$ . Figure 17 shows the extent of the  $\text{H}\alpha$ -emitters. The typical sizes correspond to a projected diameter of 6-9 kpc. The high central surface brightness favors detection by our technique. It is possible that we systematically miss the most extended objects. While all the objects are compact, they vary in morphology from almost round to noticeably elliptical ( $b/a \sim 0.5$ ). Other known high redshift galaxies are also seen to be extremely compact. Lowenthal *et al.*, 1997, report that spectroscopically confirmed  $z > 2$  galaxies in the Hubble Deep Field are seen with mean half light radii,  $\langle r_{\frac{1}{2}} \rangle = 3.6 h_{50}^{-1}$  kpc; they also report disturbed morphologies, which would not be detected at the resolution of NIRC.

Finally, we note that all of the probable star-forming objects detected have been in fields containing metal absorption-line systems, not fields at the redshift of the QSO. The only  $\text{H}\alpha$ -emitter detected at the redshift of a QSO was the Seyfert 1 in the 2149+0221 field.

## 5. Discussion and Conclusions

As discussed in MTM96, there is the possibility that all these galaxies have an active nuclear component that contributes to their line emission. We will address this suggestion before drawing conclusions from the  $\text{H}\alpha$ -emitting sample as a whole.

### Are we detecting AGN?

The observed space density of high redshift quasars is so much smaller than our space density of detections that they are very unlikely to be the same population. Warren *et al.* (1994) calculate the Luminosity Function (LF) for bright QSOs at  $z > 2$ . This LF can be used to estimate the density of active galaxies at the redshifts covered by our survey.

For bright quasars, with continuum absolute magnitudes on the AB system of  $M_c < -23$ , the space density is  $\leq 7 \times 10^{-6} / \text{Mpc}^{-3}$ . Using the evolving luminosity function suggested for the quasars, we can extend this LF down to the average magnitude for our detected objects,  $M_c \sim -19$ . This calculation predicts a density of  $2 \times 10^{-4} / \text{Mpc}^{-3}$ ; or, put another way, the QSO density predicts that we should have to observe more than 100 fields to find a single AGN. Our observed density of detections is higher than this by several orders of magnitude. If all of our objects were to prove to have active nuclei, their space density is three orders of magnitude higher than expected, so we are not simply probing the usual population of quasars that are well studied by numerous surveys.

The predicted density of AGN is more consistent, however, with that detected in the Lyman Limit searches, which typically find 10% of their objects to be AGN (as estimated from counting the number of AGNs reported in, for example, Steidel *et al.*, 1996). Our detections may be, on average, redder than the LLD galaxies, and they probably have stronger line emission (many LLD galaxies have  $\text{Ly}\alpha$  in absorption, not emission). If LLD searches were to probe the entire galaxy population at  $z > 2$ , while our survey were to be unable to find anything but AGN, one would conclude that we should arrive at a space density ten times *smaller* than the LLD searches. That is not what observations show, however, as our inferred space density may be as much as 5 times *larger* than estimates based on LLD searches.

On the other hand, our space density of objects is consistent with other searches which have been conducted for Emission Line Galaxies in the same redshift range. They, too, find clusters of ELGs. In particular, some of the rare successes of  $\text{Ly}\alpha$  searches have discovered groups of emission-line galaxies. The highest density of objects observed in a single field is the Pascarelle *et al.*, 1996a, survey which found 18  $\text{Ly}\alpha$ -emitting objects within 1  $\text{Mpc}^2$  and 300 km/s of the radio galaxy 53W002. These objects have been interpreted as “subgalactic clumps” that will collapse into a  $L^*$  or slightly larger galaxy. However, like one of the objects in the present survey, those ELGs show strong  $\text{Ly}\alpha$  emission, as well as CIV and NV in some cases. The same authors later detected similar objects in parallel HST observations (Pascarelle *et al.*, 1996b). A high density of  $\text{Ly}\alpha$ - and CIV-emitting galaxies, some up to  $L^*$ , would explain most of our detections. Francis *et al.* (1996, 1997) have detected a supercluster of  $\text{Ly}\alpha$ -emitters at  $z=2.38$ , all of which appear to have AGN characteristics in their spectra. They speculate that they are detecting a dust-reddened population of active galaxies that are the radio-quiet counterparts of the radio-galaxy population. They further suggest that they are seeing a population of galaxies undetectable in other surveys due to their red colors. While that comparison was suggested to exclude our survey based on MTM96, their I-K galaxies are not uniformly redder in I-K than objects in the present survey. We report several galaxies with  $\text{I-K} \gtrsim 4$ , while Francis reports  $\text{I-K}=3.4\text{--}5.2$  for

various objects. This allows the possibility that both surveys could be finding a similar population.

### Does the space density imply clustering?

We detect a higher density of objects than is observed either at the present day or in the LLD galaxies. We find up to  $\sim 1.2$  galaxies/sq. arcmin. in volumes that are 1 or 2% deep in redshift (though the galaxies may occupy a smaller  $\Delta z$  if they are clustered). LLD galaxies are found with a density of 0.4–0.75/sq. arcminutes, but over a much larger redshift range. We can also consider the comoving volume density. As a typical example of an LLD search, Madau *et al.* (1996) finds field galaxies with  $\langle z \rangle = 2.75$  in the Hubble Deep Field with a comoving number density of  $3.6 \times 10^{-3} \text{Mpc}^{-3}$  down to  $L^*$ . Calculating the comoving volume density of our detections yields  $0.0135^{+0.0055}_{-0.0035} \text{Mpc}^{-3}$ , a factor of 3-5 times more than the LLD galaxies. The errors are based on Poisson statistics (Gehrels 1986). The density could be higher if these galaxies are not uniformly distributed in the surveyed redshift windows; for example, if the  $\text{H}\alpha$ -emitters were as close to the absorber in the radial direction as they are in on the sky, the density could be 20 times higher. It is difficult to say whether all of these emission line galaxies would be found by the UV technique without more direct comparisons (see for example Bechtold *et al.* 1997) for  $\text{H}\alpha$  observations of a galaxy with the characteristic spectrum of a UV-selected galaxy). Alternately, we consider the density of  $\text{H}\alpha$  -emitters excluding the most likely cluster (0953+549) and excluding the Seyfert 1 (2149+02). In that case, we find a comoving density of  $0.008 \text{Mpc}^{-3}$ , still twice that of LLD galaxies, though Poisson statistics show the difference is only at the  $1.5\sigma$  level.

We can also compare our observed density of objects to the current day volume density. For example, the comoving density of present-day galaxies brighter than  $L_*$  is  $\sim 3.5 \times 10^{-4} \text{Mpc}^{-3}$  (Loveday *et al.* 1992). This comparison may only be lower limit, as there may be effects of luminosity evolution to consider. For example, Cowie *et al.* (1996) find the normalization of the luminosity function,  $\phi_*$ , approximately doubles between  $z=0.2$  and  $z=1.0$ . However, the evolution of the LF out to  $z > 2$  is highly uncertain; different analysis of the Hubble Deep Field data set produce very different LFs (see Bershadsky *et al.* 1997 and the references therein). We adopt as a second standard of comparison, the luminosity function of Sawicki, Lin & Yee (1997; SLY) which has two magnitudes of evolution in  $L_*$  at  $2 < z < 3$  and a steeper faint end slope in that redshift range. SLY predict a factor of  $\sim 3$  more galaxies down to today's  $L_*$ , or a comoving density of  $1.2 \times 10^{-3} \text{Mpc}^{-3}$  at  $\langle z \rangle = 2.5$ .

If all our candidate galaxies are confirmed, it could imply that we are seeing clustering

in the environments of metal absorption line systems. Even if the ELGs are all AGN, it would be unusual to find so many.

If we consider clustering to be a possibility, we must examine two cases – either the galaxies are in a cluster, or they are simply correlated on the large redshift scales at which we are observing. In the first case, we assume that the galaxies are at nearly identical redshifts. Specifically, we assume that they are as close in redshift as they are in projected distance, which increases our space density of detected objects by a factor of  $\sim 20$ . Under this assumption, we compare our comoving density to the current day comoving density and we find that on the scale of a cubic NIRC field the correlation function,  $\xi(0.3Mpc)$ , is 5 times its present value (not accounting for possible evolution) or  $\sim 1.5$  times the value implied by SLY at the same redshift. We note that this comparison may be an lower limit on how strongly clustered the galaxies are, if there is a gravitational effect that reduces how much the cluster expands relative to the Hubble expansion. In the second case we assume that the galaxies we detect are uniformly distributed along redshift in the window sampled by the narrowband filter. In this case, we consider a radius equal to half of the long side ( $\delta z$ ) of our highly rectangular search window. Comparing our comoving density to the current day, the correlation function inside that comoving volume,  $\xi(3.25Mpc)$  is then 15 times the current value (where we assume  $\xi_{current} \propto (r/5Mpc)^{-1.77}$ , Peebles 1973) or 5 times the value inferred from SLY.

The inferred clustering of our galaxies is somewhat stronger than what is seen between the quasar metal absorption-line systems themselves. Absorption systems have been seen to be correlated on radial scale corresponding to our  $\Delta z$  windows. Sargent, Boksenberg, & Steidel (1988) see  $\xi = 5$ –10 for CIV absorbers at scales from 200 to 600 km/s. Similarly, Steidel & Sargent (1992) see correlations of  $\xi(600 \leq \Delta v \leq 5000km/s) = 2.6$ , for MgII absorbers at redshifts of  $0.6 < z < 2.2$ . Our narrowband filters with  $\Delta z/z = 1\%$ , probe velocity differences on the order of several times  $10^3$ km/s, so we may see more clustering on this scale than is expected for absorbers.

On the other hand, the density we find seems to be consistent with surveys of QSO environments at high redshift. Ellingson *et al.* (1991) find that the richest environments of radio loud QSOs at  $z \sim 0.5$  are well fit by the Schechter parameters  $\Phi = 6.5/Mpc^2$  and  $M_r^* = -22.6$ , assuming  $\alpha = -1.0$ . This predicts that down to  $L^*$  we should see 0.6 excess galaxies per comoving  $Mpc^2$ . In our case, we see  $\sim 0.4$  galaxies per comoving  $Mpc^2$ . Hall & Green (1998) find several radio-loud QSOs at  $z \sim 1.5$  reside in apparent rich clusters, detected as an excess of red (in r-K) objects. Their models suggest these clusters are consistent with  $z_{form} > 4$ , similar to the conclusions in MTM96. Hutchings, 1995, finds an excess of galaxies around QSOs at  $z = 2.3$ . These counts are attributed to compact groups

of starburst galaxies. The detected excess galaxies, down to  $R=24$ , is 30–84 per  $\text{Mpc}^2$ . While Hutchings’ counts are not spectroscopically confirmed, they do suggest the presence of clustering at high redshifts, at least in quasar environments.

## Reddening

We note that reddening could also explain the potential difference in density between LLD searches and our candidate ELGs. However, to reconcile the number counts with *no* clustering, we would need  $\langle E_{B-V} \rangle$  to be sufficiently large to make galaxies with  $\text{SFR} \sim 30 M_{\odot}/\text{yr}$  unobservable spectroscopically in the optical. Depending on the reddening law, this requires  $\langle E(B-V) \rangle \sim 0.7 - 0.9$  mag. This amount of extinction seems incompatible with the observed g-R colors of the LLD galaxies, for any reasonable extinction law (Fitzpatrick 1986, Calzetti *et al.* 1994, etc.)

Even if the observed densities of LLD galaxies and  $\text{H}\alpha$ -emitters are similar (if, for example, our marginal detections prove false) reddening is still important in understanding the nature of these high redshift galaxies. In particular, consider the SFR determined from our best candidates. Even assuming (as a worst case) that there is a small (30%) AGN contribution to the line flux, we infer an average  $\text{SFR} \gtrsim 35 M_{\odot}/\text{yr}$ . This SFR is large compared to the uncorrected average SFR of the LLD galaxies (Steidel *et al.* 1996, Lowenthal *et al.* 1997)), as derived from the UV continuum. More recent estimates from the LLD galaxies (*cf.* Pettini *et al.* 1997) give a factor of 3–5 redding correction, which brings the LLD average within a factor of two of ours. We can also contrast our  $\text{H}\alpha$  star formation rates with those inferred from  $\text{Ly}\alpha$  selected objects. Cowie & Hu (1998) present a dozen  $\text{Ly}\alpha$ -emitters, which would have a maximum  $\text{SFR}=10 M_{\odot}/\text{yr}$ , in the absence of extinction.

In summary, we have shown that with the Keck telescope the narrow-band near-IR search technique for emission-line galaxies at  $z > 2$  provides an effective means of detecting groups of star forming galaxies. We detect galaxies with a high comoving volume density, suggesting that it is unlikely that the line and continuum emission from these objects is dominated by active nuclei. The density further suggests that we observe clustering in the environment of metal-line absorbers. The inferred star-formation rates of these galaxies agree well with de-reddened estimates for UV-selected galaxies at similar redshifts.

We thank the Observing Assistants and Instrument Specialists at the Keck telescopes, especially B. Schaefer, R. Quick, T. Stickle, T. Bida, R. Cambell, B. Goodrich, and W. Harrison. Data presented herein were obtained at the W.M. Keck Observatory, which is operated as a scientific partnership among the California Institute of Technology, the

University of California and the National Aeronautics and Space Administration. The Observatory was made possible by the generous financial support of the W.M. Keck Foundation. This research has made use of the NASA/IPAC Extragalactic Database (NED) which is operated by the Jet Propulsion Laboratory, California Institute of Technology, under contract with the National Aeronautics and Space Administration.

## REFERENCES

- Bechtold, J., Yee, H.K.C., Elston, R., & Ellingson, E., 1997, ApJL, 477, 29
- Bershady, M.A., Majewski, S.R., Koo, D.C, Kron, R.G., & Munn, J.A., 1997, ApJ, 490, L41
- Bertin, E. & Arnouts, S., A&AS, 1996, 117, 393
- Calzetti, D.A., Kinney, A.L., & Storchi-Bergmann, T., 1994, ApJ, 429, 482
- Carballo, R., Barcons, X., & Webb, J.K., 1995, AJ, 109, 1531
- Cowie, L.L, Songaila, A., Hu, E.M., & Cohen, J.G., 1996, AJ, 112, 839
- Cowie, L.L. & Hu, E.M., 1998, in press in ApJ
- Ellingson, E., Yee, H.K.C., & Green, R.F., 1991, ApJ, 371, 49
- Fitzpatrick, E.L., 1986, AJ, 92, 1068
- Francis, P.J., *et al.*, 1996, ApJ, 457, 490
- Francis, P.J., Woodgate, B.E., & Danks, A.C., 1997, ApJL, 482,25
- Gehrels, N., 1986, ApJ, 303, 336
- Hall, P.B., & Green, R.F., 1998, *in press*
- Hazard, C., Morton, D.C., McMahon, R.G., Sargent, W.L.W, & Terlevich, R., 1986, MNRAS 223, 87
- Howell, S.B., 1989, PASP, 101, 616
- Hutchings, J.B., 1995, AJ, 109, 1541
- Kennicutt, R. 1983, ApJ 272, 54
- Kron, R.G. 1980, ApJS 43, 305
- Levshakov, S. A. 1992, AJ 104, 950
- Loveday, J., Peterson, B.A., Efstathiou, G., Maddox, S.J., 1992, ApJ, 390, 338
- Lowenthal, J.D. *et al.*, 1997, ApJ, 481, 673

- Madau, P., Ferguson, H.C., Dickinson, M.E., Giavalisco, M., Steidel, C.C., Fruchter, A., 1996, MNRAS, 283, 1388
- Malkan, M., Teplitz, H., & McLean, I., 1995, ApJ Letters 448, L5 (MTM95)
- Malkan, M., Teplitz, H., & McLean, I., 1996, ApJ Letters 468, L9 (MTM96)
- Maoz *et al.*, 1993, ApJ 409, 28
- McLean, I.S. & Teplitz, H., 1996, AJ, 112, 2500
- Matthews, K., & Soifer, B. T. 1994, in *Infrared Astronomy with Arrays: The Next Generation*, ed I. McLean (Dordrecht:Kluwer), 239
- Oke, J. B., *et al.*, 1995, P.A.S.P, 107, 375
- Osmer, P.S., Porter, A.C., & Green, R.F., 1994, ApJ 436, 6780
- Pahre, M.A. & Djorgovski, S.G., 1995, ApJL, 449, 1
- Pascarelle, S.M., Windhorst, R.A., Keel, W.C., & Odewahn, S.C., 1996a, Nature, 383, 45
- Pascarelle, S.M., Windhorst, R.A., Keel, W.C., Scoville, N., Armus, L., 1996, BAAS, 189, 83.02
- Peebles, P.J.E., 1993, *Principles of Physical Cosmology*, Princeton University Press, Princeton, New Jersey
- Pettini, M., Steidel, C., Dickinson, M., Kellogg, M., Giavalisco, M., Adelberger, K., 1997, in ‘The Ultraviolet Universe at Low and High Redshift’, ed. W. Waller, (Woodbury: AIP Press)
- Sargent, W.L.W., Boksenberg, A., & Steidel, C.C., 1988, ApJS, 68, 539
- Sawicki, M.J., Lin, H., & Yee, H.K.C, 1997, AJ, 113, 1
- Schneider, D.P, Schmidt, M., & Gunn, J.E., 1994, AJ107, 1245
- Steidel, C.C., & Sargent, W.L.W., 1992, ApJS, 80, 1
- Steidel, C.C., Giavalisco, M., Pettini, M., Dickinson, M., & Adelberger, K.L., 1996, ApJ Letters 462, L17
- Thompson, D., Djorgovski, S, & Trauger, J., 1995, AJ, 110, 963
- Trager, S.C., Faber, S.M., Dressler, A., & Oemler, A., 1997, ApJ, 485, 92
- Vogel, S. & Reimers, D., 1995, A&A, 294, 377
- Warren, S.J., Hewett, P.C., & Osmer, P.S., 1994, ApJ, 421, 412
- Wainscoat, R.J. & Cowie, L.L., 1992, AJ, 103, 332

Yee, H.K.C., Ellingson, E., Bechtold, R.G., Carlberg, R.G., Cuillandre, J.-C., 1996, AJ111, 1783

York, D.G., Yanny, B., Crotts, A., Carilli, C., & Garrison, E., 1991, MNRAS, 250, 24

Table 1. Transmission of NIRC Filters

Filter	central $\lambda$ ( $\mu\text{m}$ )	$\Delta\lambda/\lambda$ (%) <sup>a</sup>	$z$ for $\text{H}\alpha$ <sup>b</sup>	$1/(\text{T:K}')$ <sup>c</sup>
H2(1–0)	2.12	1.1	2.23	40
Br $\gamma$	2.16	1.0	2.29	24.0
H2(2–1)	2.24	1.0	2.41	40
K continuum	2.26	2.3	2.44	7.5
CO(2–0)	2.30	1.2	2.50	19.0

<sup>a</sup> $\Delta\lambda$  is defined to be the FWHM of the filter tracing.

<sup>b</sup>The filter admits a range of  $z$ , corresponding to the redshifted FWHM limits

<sup>c</sup>The transmission relative to  $\text{K}'$

Table 2. Targets

Field	$z$	type	date	$t_{K'}$	$t_{n.b.}$
LBQS 0059-0207	2.300	R.Q.	10/12/95	1080	4320
Q 0114-089	2.2995	CIV <sup>h</sup>	01/15/98	1620	4320
Q 0149+335	2.431	R.L.	07/18/94	1080	2070
Q0153+045 (NW)	2.4243	CIV <sup>a</sup>	01/02/96	1080	4050
Q0153+045 (center)	2.423	CIV	11/18/96	1620	4860
Q0201+365	2.460,2.4241	CIV,SiII,FeII,AlIII <sup>a</sup>	10/13/95	1620	5400
Q0216+080	2.2931	CIV <sup>a</sup>	07/18/94	540	2400
G0727+4056	2.500	R.L. <sup>b</sup>	11/18/96	1620	6480
SBS0747+611	2.487,2.4865	assoc. <sup>c</sup>	01/02/96	1080	4320
Q0846+156	2.28	CIV <sup>a</sup>	01/13/95	2160	6480
SBS0953+549 (SE)	2.50	CII,NV <sup>d</sup>	01/13/95	1620	3600
SBS0953+549 (SE)	2.449	OVI,SiIII	01/13/95	1620	2700
SBS0953+549 (NW)	2.50	CII,NV	01/02/96	540	3120
SBS0953+549 (SW)	2.50	CII,NV	11/18/96	1080	4320
SBS0953+549 (NE)	2.50	CII,NV	01/14/98	1980	6480
SBS0953+549 (SSE)	2.50	CII,NV	01/14-15/98	1380	6960
SBS0953+549 (EE)	2.50	CII,NV	01/15/98	1680	6240
SBS0953+549 (WW)	2.50	CII,NV	01/15/98	1200	6000
LBQS 1240+1516	2.297	R.Q.	3/25/97	1620	2160
[CCSS 1332+261]	2.498	CIV <sup>g</sup>	3/25/97	1620	4320
SP89 1442+295	2.439	CIV,CII,OI <sup>e</sup>	06/27/96	1080	4650

Table 2—Continued

Field	$z$	type	date	$t_{K'}$	$t_{n.b.}$
Q1623+268	2.490	R.Q.	06/28/96	1620	6480
HS 1700+6416	2.290,2.308	OIII,CII <sup>f</sup>	06/27/96	1440	4320
Q1726+344	2.2992	HI <sup>g</sup>	06/28/96	1620	3600
PC 2149+0221	2.304	R.Q.	10/13/95	1080	4320
Q 2233+131	2.4915	CIV <sup>a</sup>	07/16/94	630	1440
Q2343+125	2.4285,2.4308	CIV,AIII,FeII,SiII <sup>h</sup>	07/19/94	540	1400
Q2344+125	2.4265,2.4292,2.4371	CIV <sup>h</sup>	06/27-28/96	2160	5400
Q2348-011	2.4272	DLA <sup>a</sup>	11/18/96	1440	4860
Q2349+002 (NE)	2.495	R.Q.	10/12-13/95	1620	4320

Note. — R.L. = emission redshift of Radio Loud QSO; R.Q. = emission  $z$  of Radio Quiet QSO

<sup>a</sup>Sargent, Steidel, & Boksenberg, 1989

<sup>b</sup>Owen, Ledlow, & Keel, 1995

<sup>c</sup>Steidel & Sargent, 1992

<sup>d</sup>Levshakov, 1992

<sup>e</sup>Carballo, Barcons, & Webb, 1995

<sup>f</sup>Vogel & Reimers, 1995

<sup>g</sup>Junkkarinen, Hewitt, & Burbidge, 1991

<sup>h</sup>Sargent, Boksenberg, & Steidel, 1988

Table 3. Detections

Object	$\Delta$ m	Line Flux <sup>a</sup>	E.W. (rest Å)	K'	H	J	I	V	B
Q0114 A	0.27	249	29	15.42	...	...	...	19.8 <sup>a</sup>	...
Q0114 B	1.0	15.4	151	20.3	...	...	...	...	...
Q0153+045 A	0.8	6	126	21.1	...	$\geq 23$	24.9	$\geq 25.2$	...
Q0846+156 A	1.4	5	264	22.1	...	...	...	...	...
SBS0953+549 A	1.0	25	119	19.7	20.5	21.7	23.7	24.57	24.7
SBS0953+549 B	2.4	26	639	21.55	:22	23.09	24.53	25.2	24.8
SBS0953+549 C	1.7	8.6	298	21.76	:22	22.35	24.04	24.65	25.2
SBS0953+549 D	1.7	14.4	360	21.33	...	...	23.5	24.16	24.8
SBS0953+549 E	1.4	9.2	250	21.42	...	...	25.08	25.46	26.2
SBS0953+549 F	0.5	13.9	54	19.34	...	...	24.47	25.83	:27
HS 1700+6416 A	0.5	8.3	58	19.9	...	21.6	...	...	...
HS 1700+6416 B	0.75	8.9	100	20.4	...	23.8	...	...	...
PC 2149+0221 A	0.9	580.5	85	18.15	18.4	19.00	...	...	...

<sup>a</sup> $10^{-17}$ ergs/cm<sup>2</sup>/s

Table 4. QSO Photometry

QSO	$z$	optical magnitude <sup>a</sup>	$K'$
LBQS 0059-0207	2.300	18.40	15.00
Q 0114-089	3.157	17.4	15.4
Q 0149+335	2.431	18.5	15.98
Q0153+045	2.991	18.8	15.26
Q0201+365	2.912	17.5	16.13
Q0216+080	2.991	18.1	15.52
SBS0747+611	2.487	17.5	15.29
Q0846+156	2.928	18.3	15.63
SBS0953+549	2.584	17.5	15.30
LBQS 1240+1516	2.297	18.3	16.23
[CCSS 1332+261]	2.503	18.6	15.4
SP89 1442+295	2.638	17	14.00
Q1623+268	2.490	18	16.34
HS 1700+6416	2.722	16.1	14.05
Q1726+344	2.430	18.5	16.18
PC 2149+0221	2.304	18.39	16.64
Q 2233+131	3.274	18.8	15.66
Q2343+125	2.515	...	13.37
Q2344+125	2.763	18.0	...
Q2348-011	3.014	18.0	16.32
Q2349+002	2.495	19.90	15.0

<sup>a</sup>from the NED catalog (see references therein)

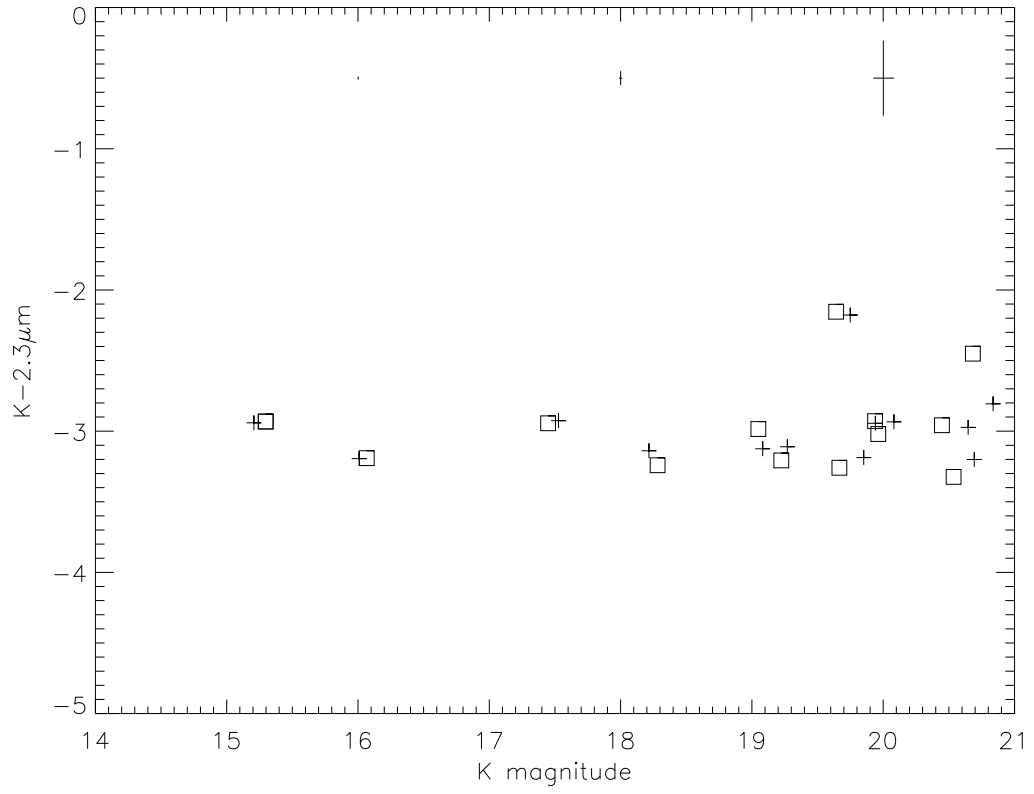


Fig. 1.— A comparison of the broad-minus-narrow colors measured by aperture photometry (+ symbols) and by gaussian fitting (squares) for our first detection (see MTM95). Typical  $1\sigma$  errors are shown at the top.

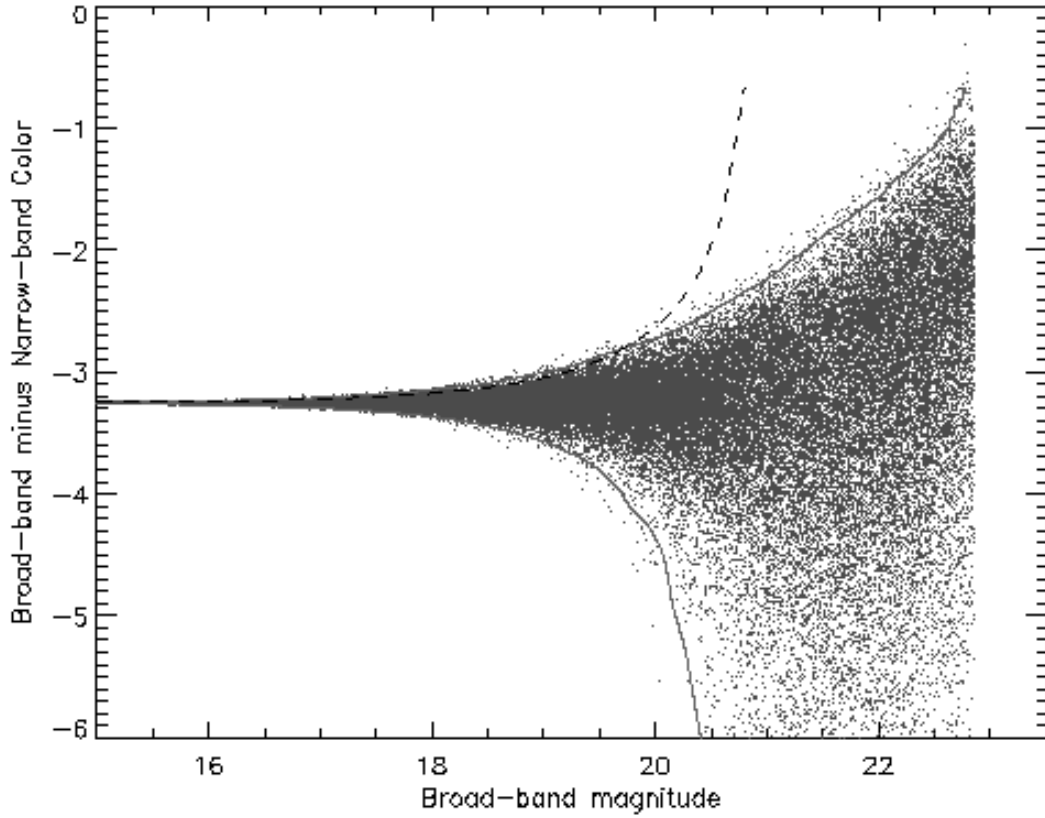


Fig. 2.— Simulated color-magnitude diagram for 100,000 objects with a constant broad-band to narrow-band flux ratio of 20 and typical photometric errors. The dark lines indicate the 99.5% confidence intervals above and below the mean. The sharp cutoff at the faint end of the broad-band scale is located at the  $1\sigma$  broad-band detection limit. The dashed line indicates the less accurate, first order approximation of the  $3\sigma$  errors.

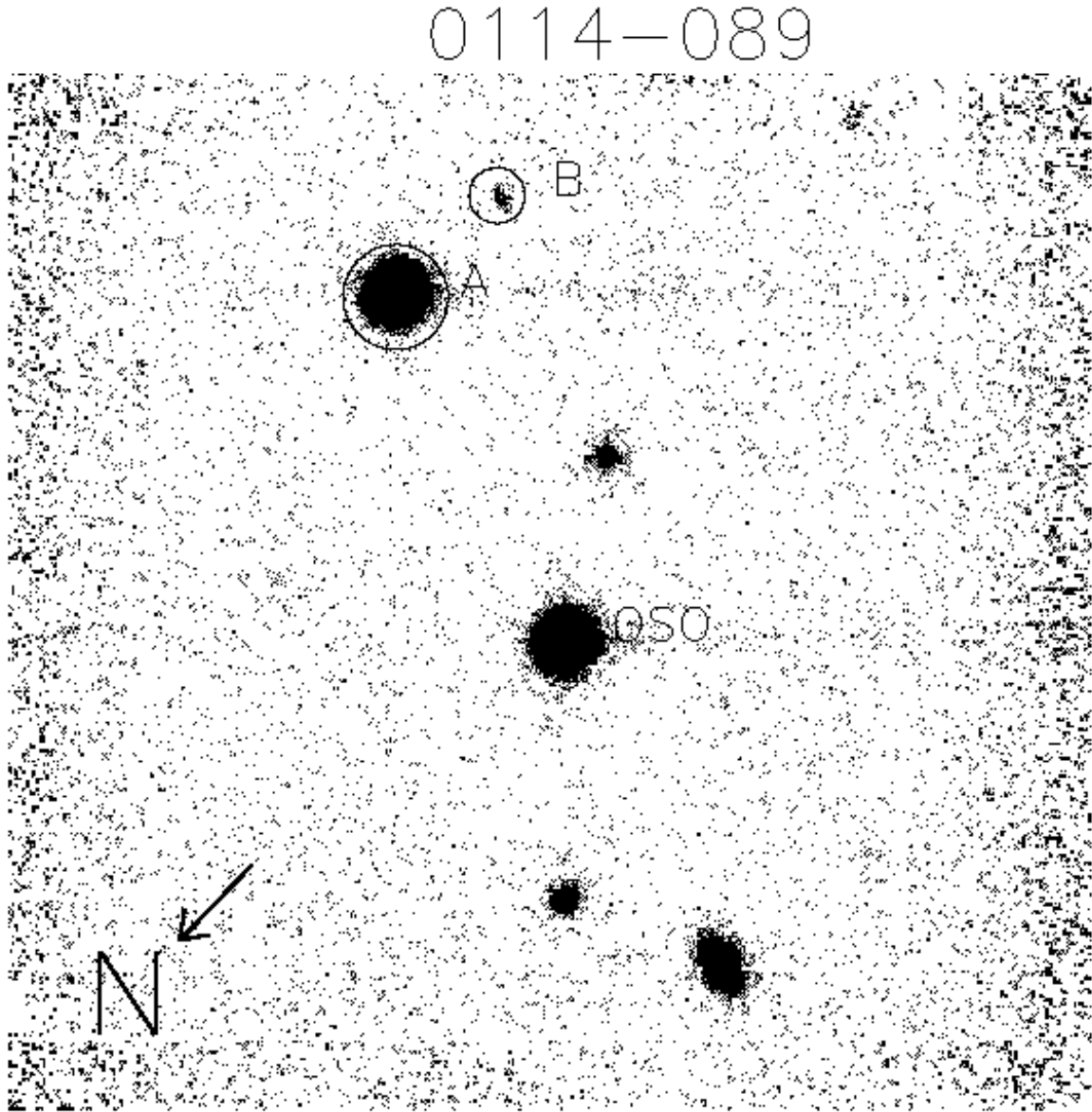


Fig. 3.—  $46.5 \times 44.4''$  K' image of the 0114-089 field. The emission line objects are indicated as A and B.

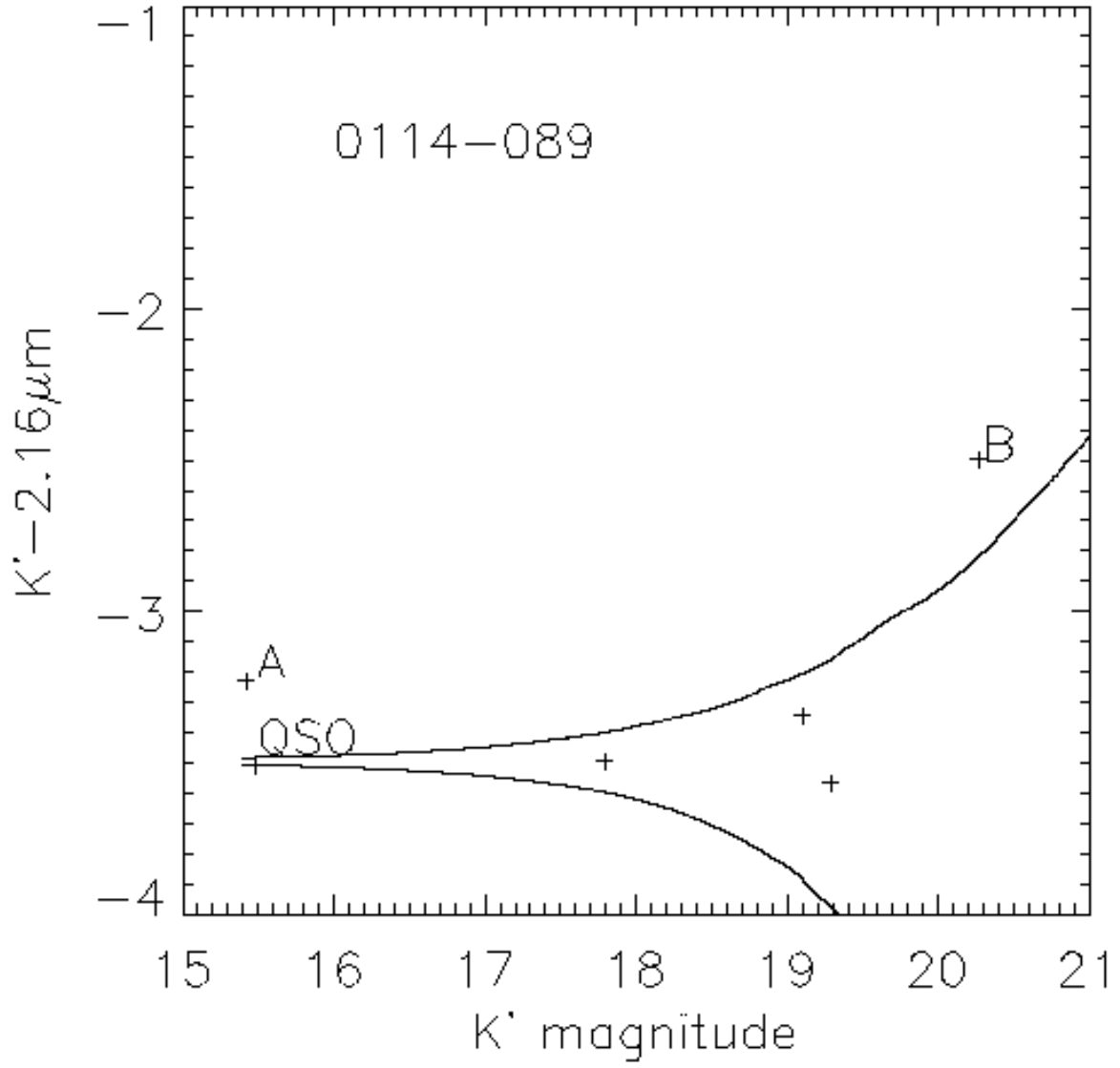


Fig. 4.—  $(K'-Br\gamma$  vs.  $K'$  for the 0114-089 field. The curves lines indicate the  $3\sigma$  confidence interval.

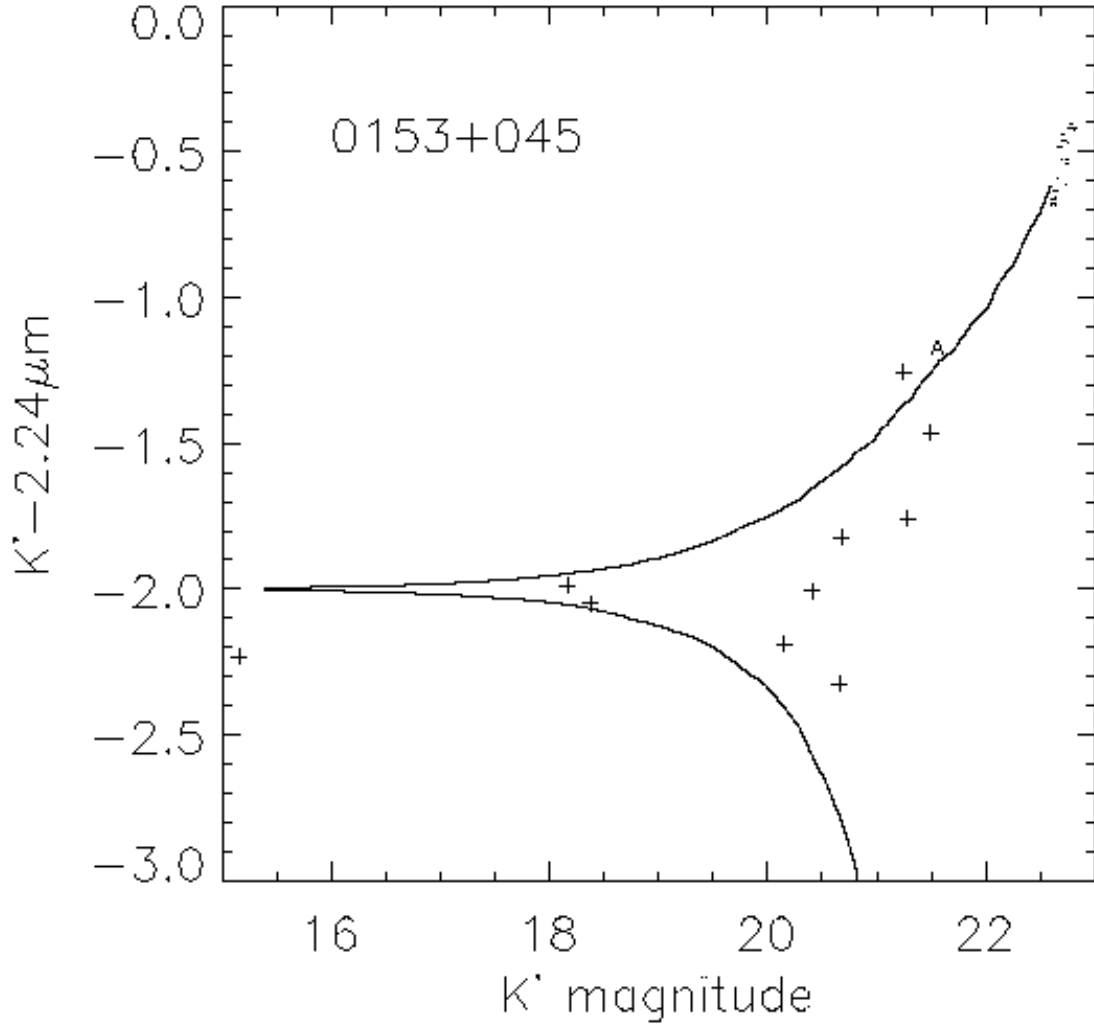


Fig. 5.—  $(K'-K_{\text{con}})$  vs.  $K'$  for the 0153+045 field. The curved lines indicate  $3\sigma$  errors.

0153+045

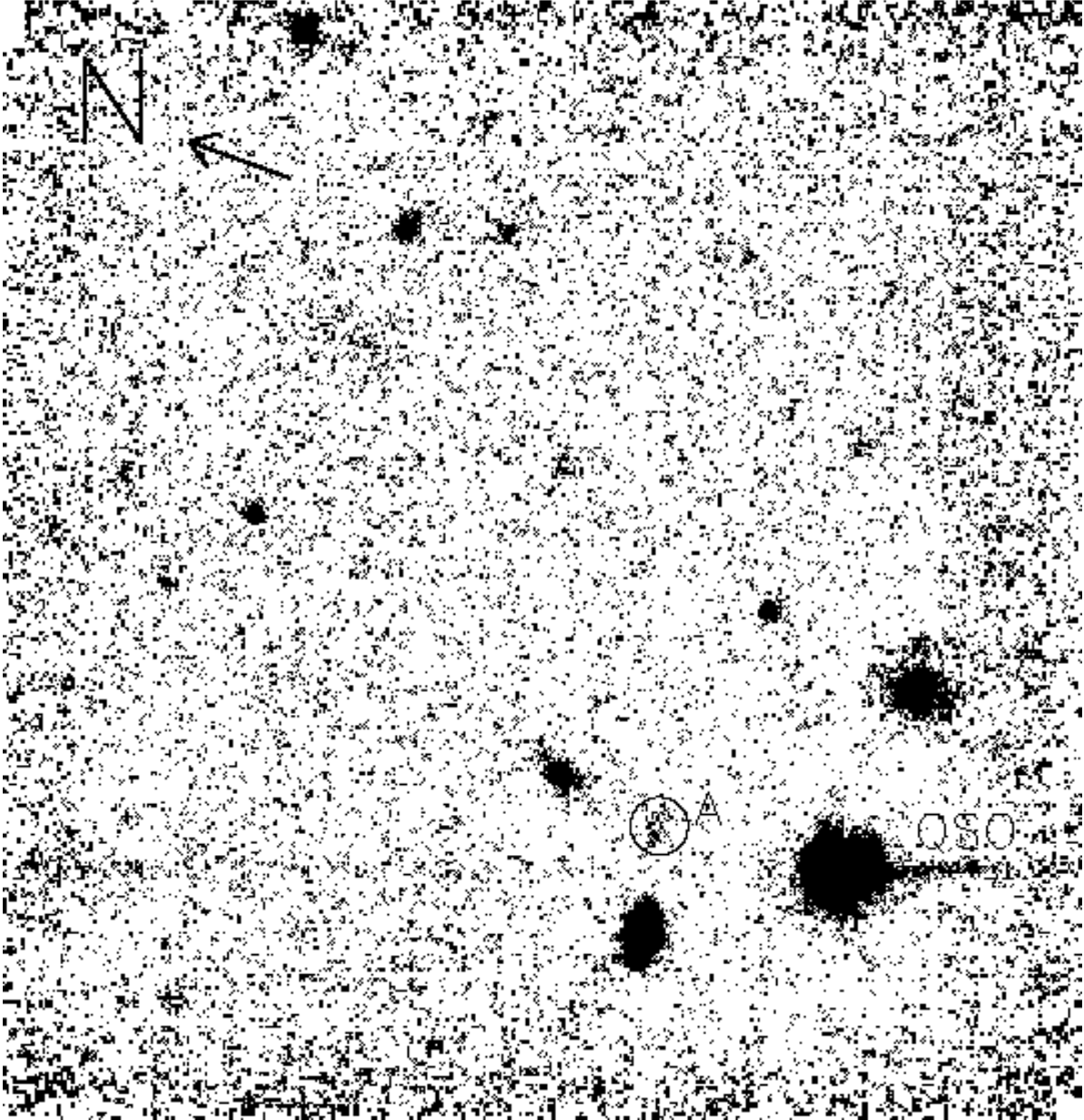


Fig. 6.—  $47'' \times 48''$   $K'$  image of the 0153+045 field. The “trail” from the bright QSO is an artifact of the readout electronics.

0846+156

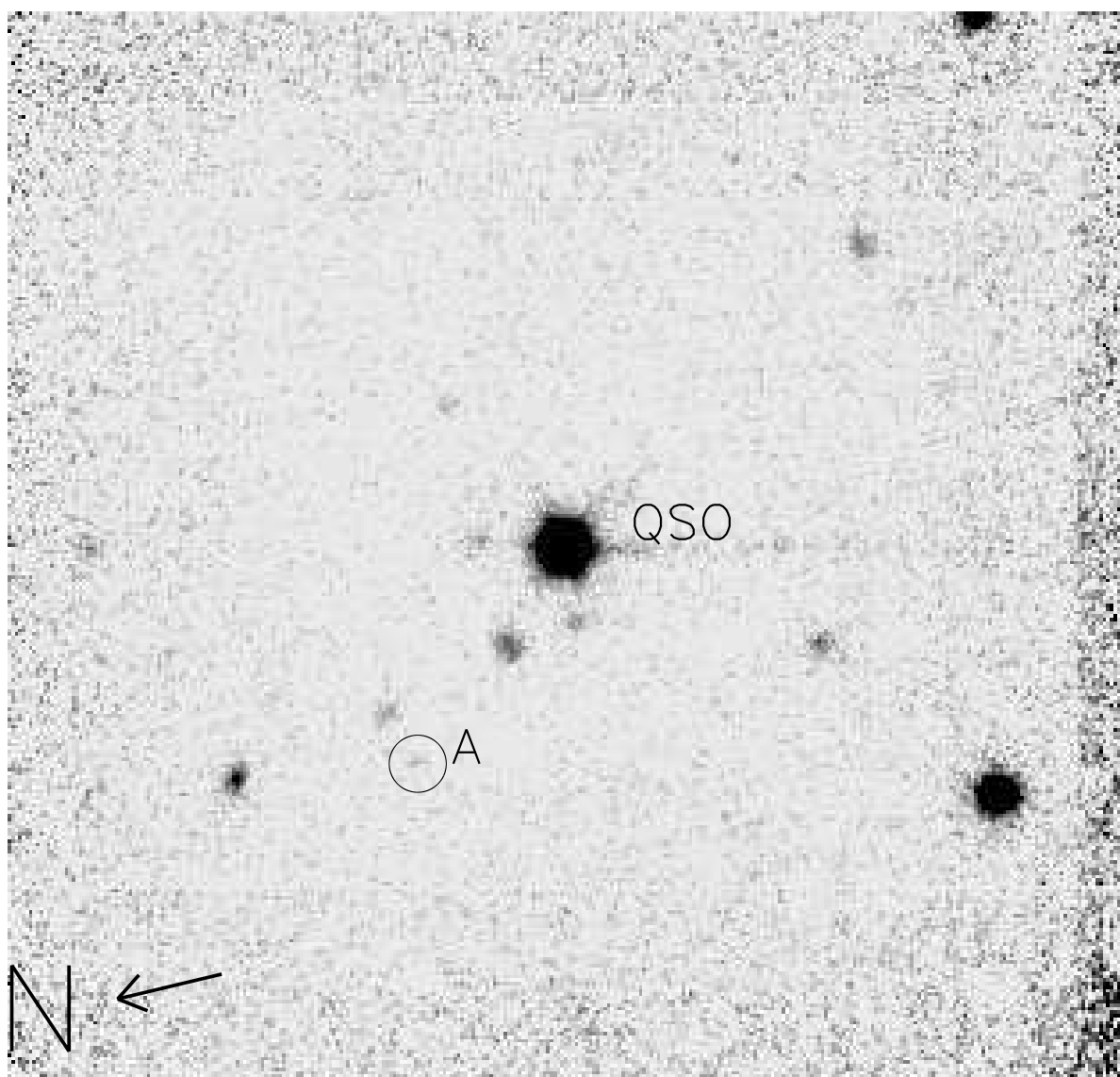


Fig. 7.— The  $47'' \times 45''$   $K'$  image of the 0846+156 field.

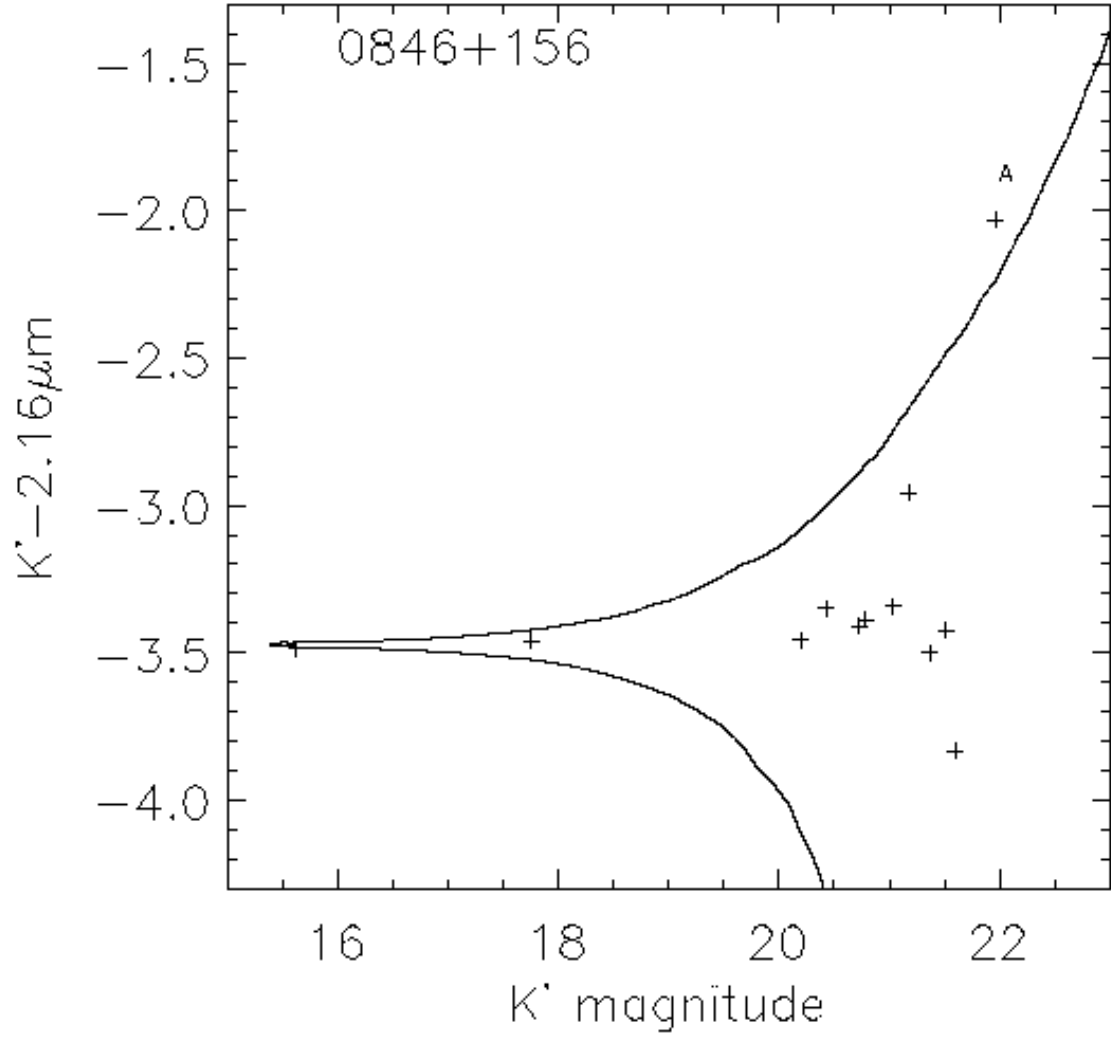


Fig. 8.— (K'-Br $\gamma$ ) vs. K' for the 0846+156 field. The curved lines indicate the  $3\sigma$  errors.

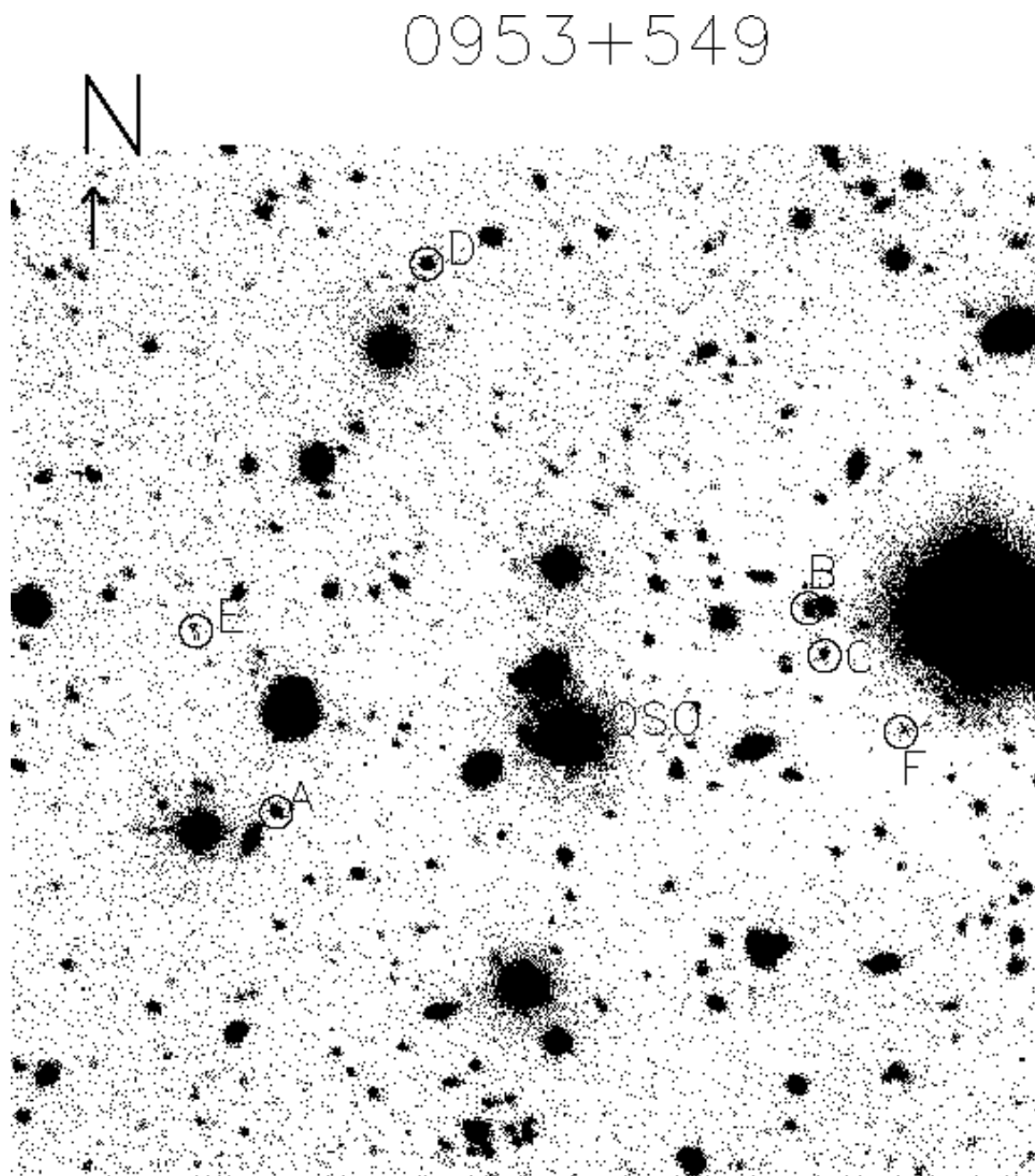


Fig. 9.— I band image of the 0953+549 field.

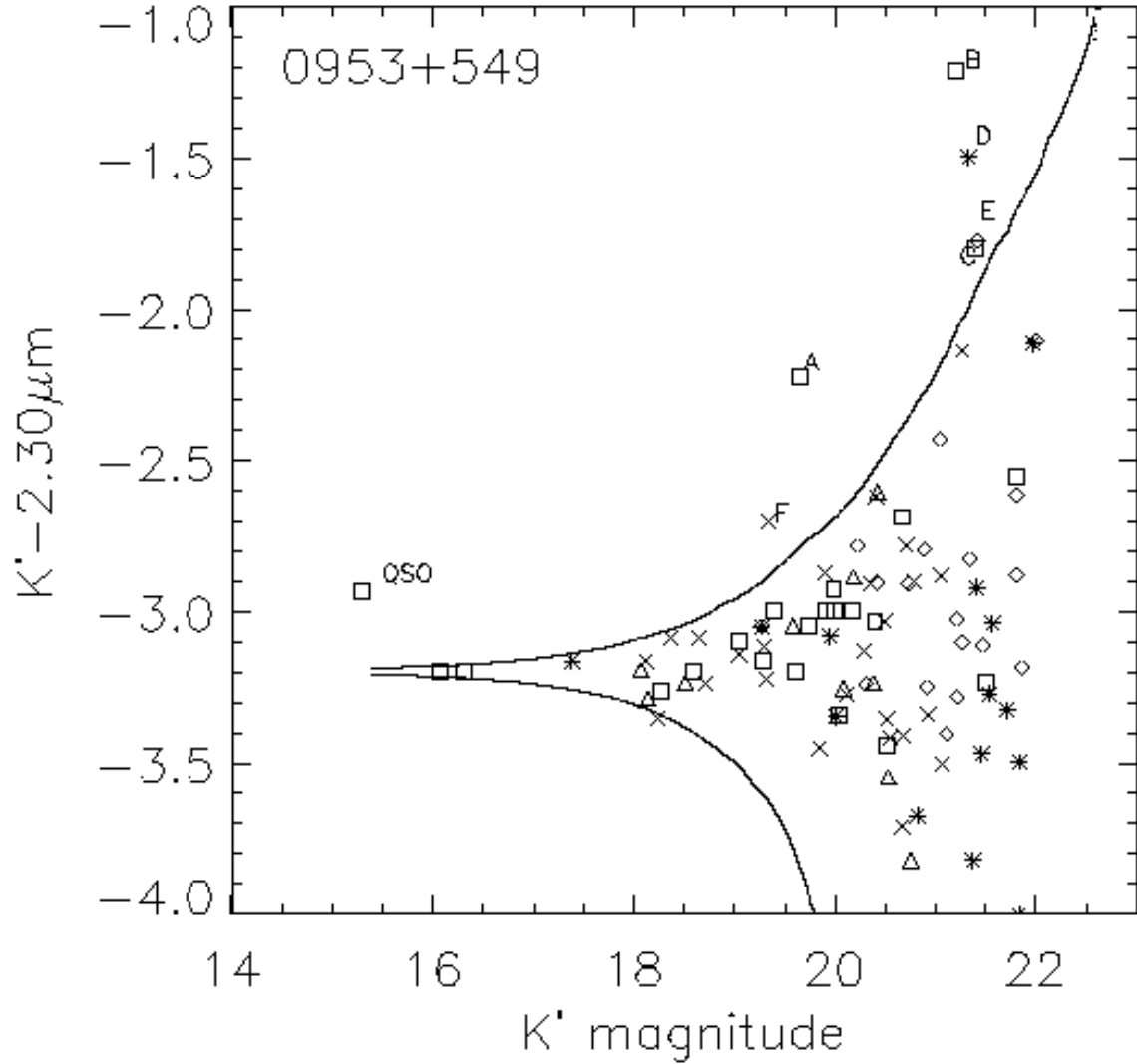


Fig. 10.—  $(K' - 2.30 \mu\text{m})$  vs.  $K'$  for the 0953+549 field. The curved lines indicate  $3\sigma$  errors. The squares indicate data that appeared in MTM95 and MTM96. The crosses indicate objects in the NIRC field SE of the QSO. The \* symbols indicate objects in the NIRC field NE of the QSO. The diamonds indicate objects that are in the NIRC field east of MTM095355+545428.

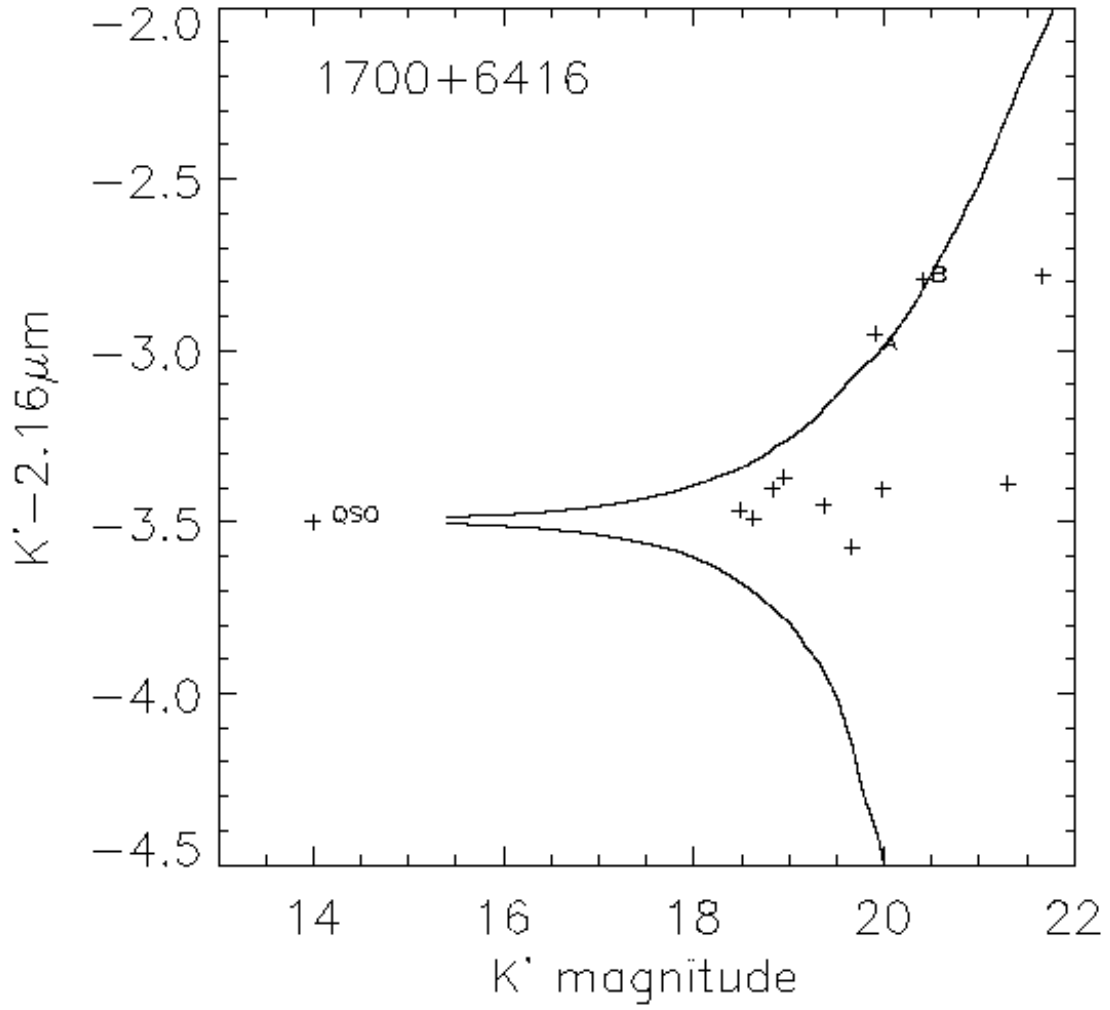


Fig. 11.—  $(K' - 2.16 \mu\text{m})$  vs.  $K'$  for the 1700+6416 field. The curved lines indicate  $3\sigma$  errors.

1700+6416

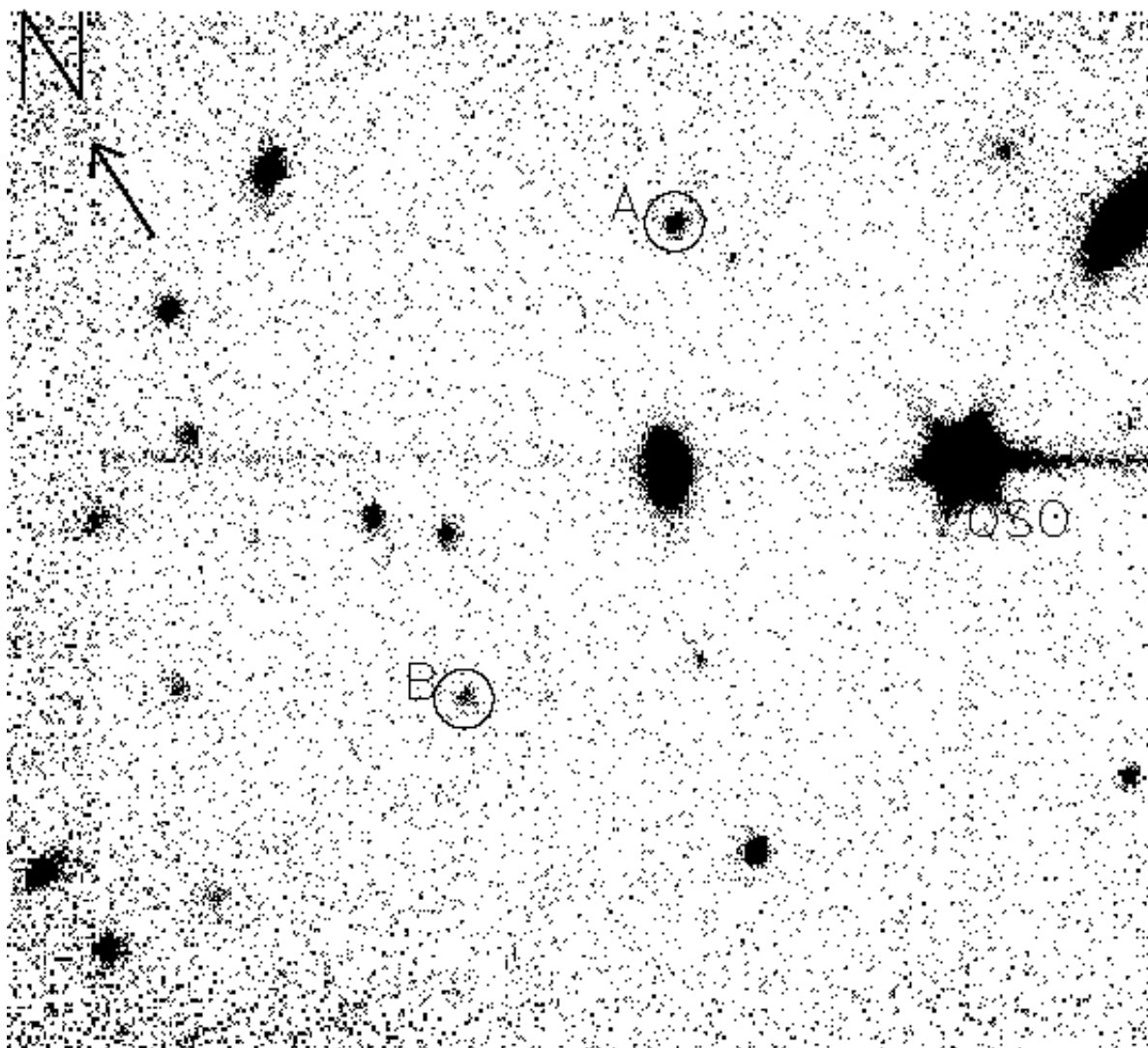


Fig. 12.—  $45'' \times 47''$   $K'$  image of the 1700+6416 field.

2149+021

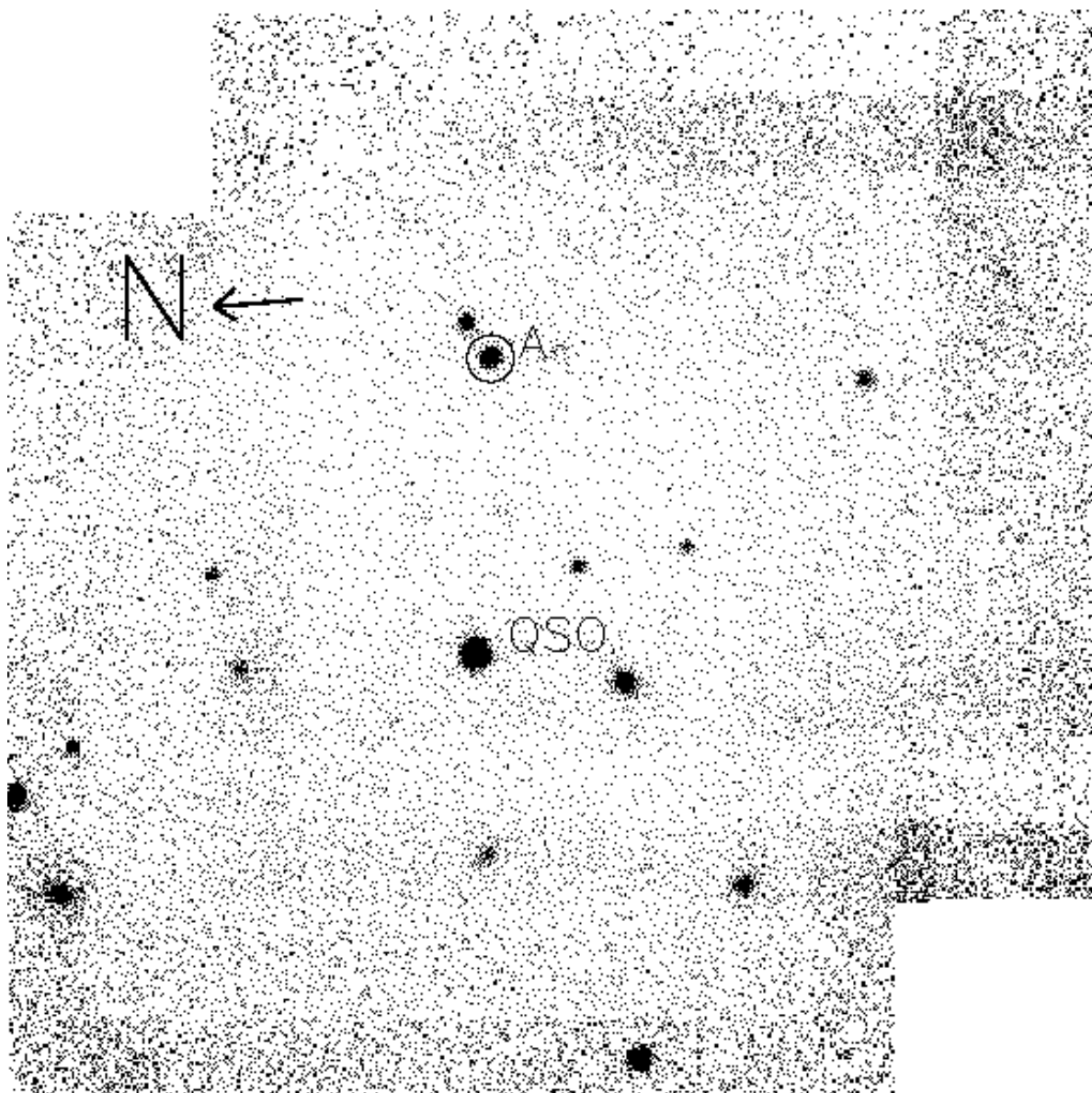


Fig. 13.—  $36'' \times 39''$   $K'$  image of the 2149+0221 field.

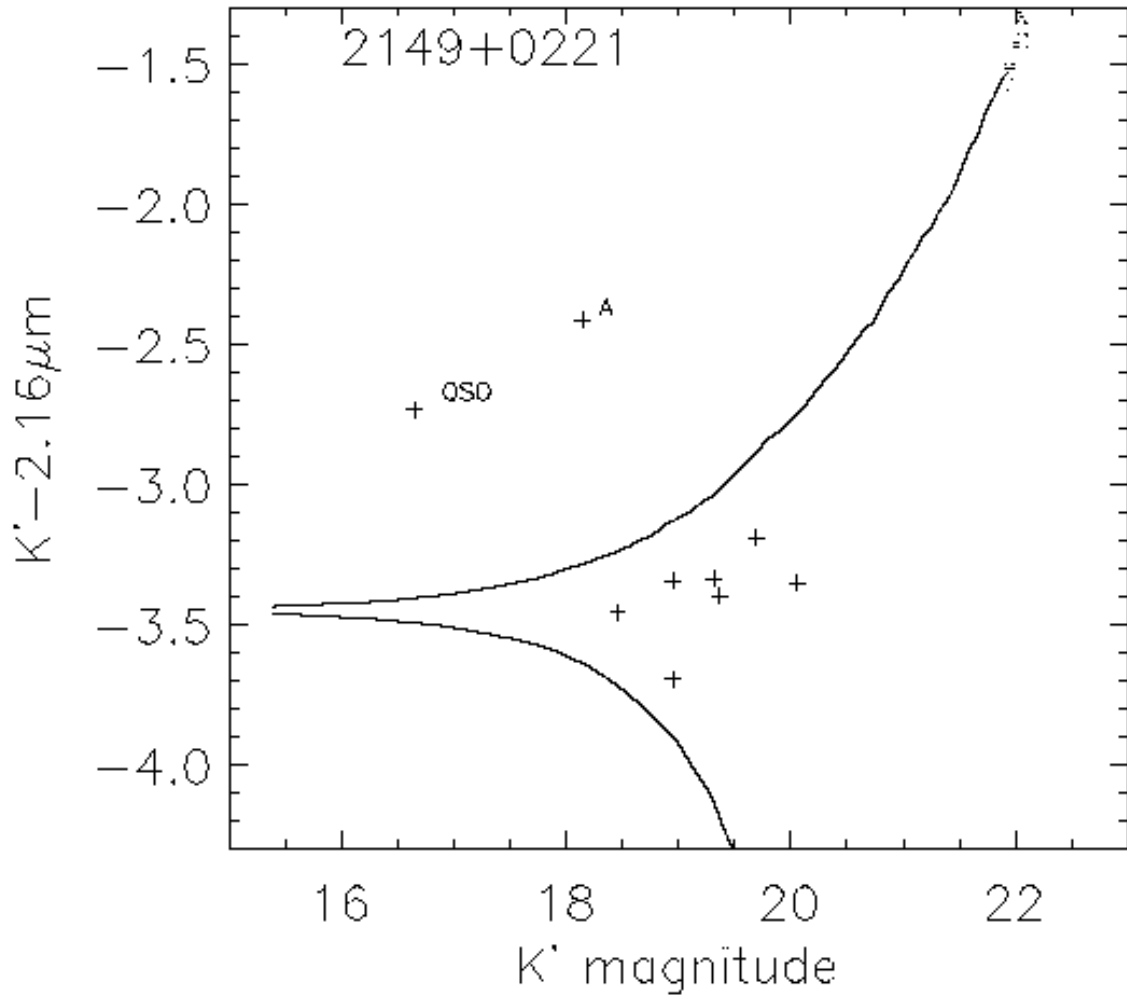


Fig. 14.—  $(K' - 2.16 \mu\text{m})$  vs.  $K'$  for the 2149+0221 field. The curved lines indicate  $3\sigma$  errors.

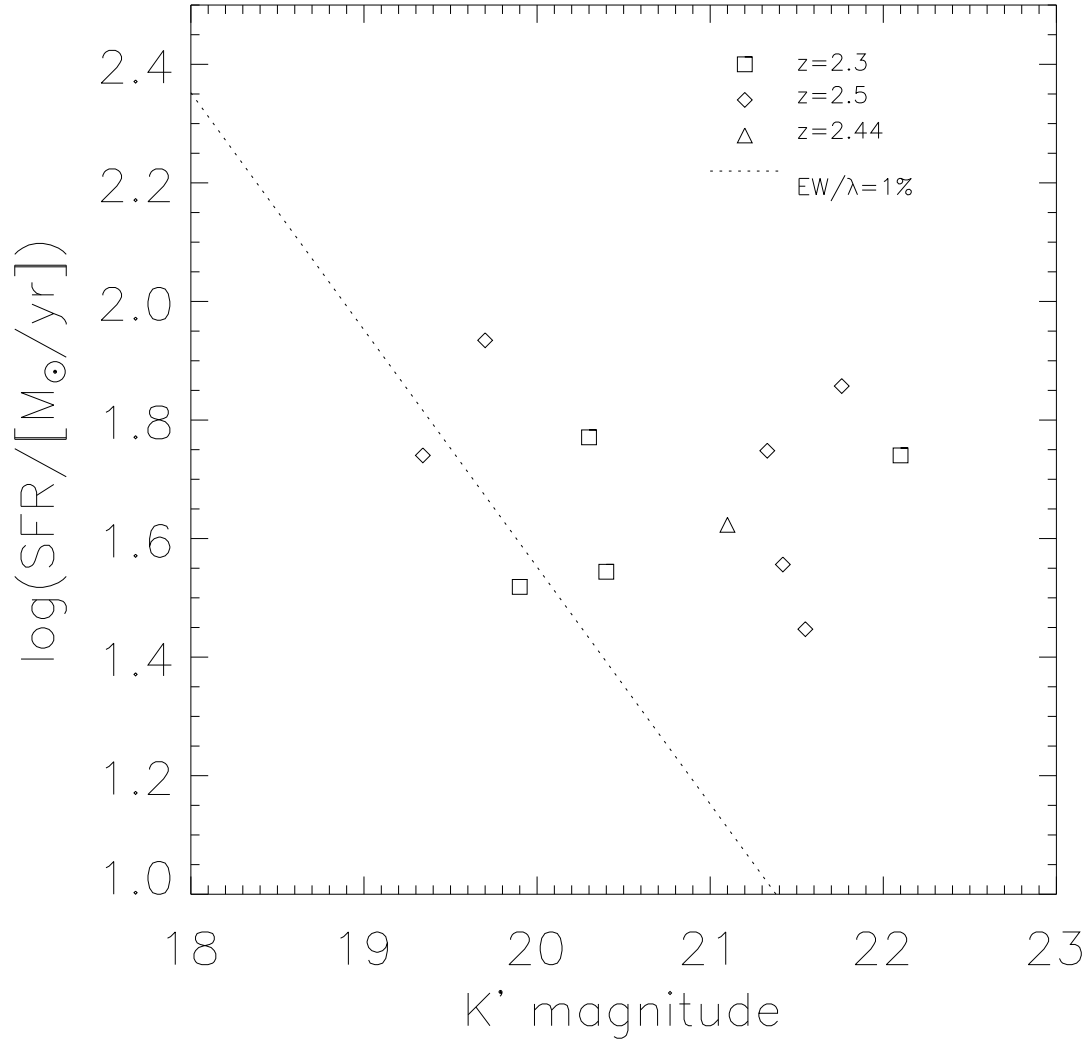


Fig. 15.— Star Formation Rates of H $\alpha$  emitters vs. K' magnitudes. The squares show objects detected in the Br $\gamma$  filter, the diamonds objects in the CO filter, and triangles objects in the K-continuum filter. The diagonal line indicates constant  $\text{EW}/\lambda=0.01$ .

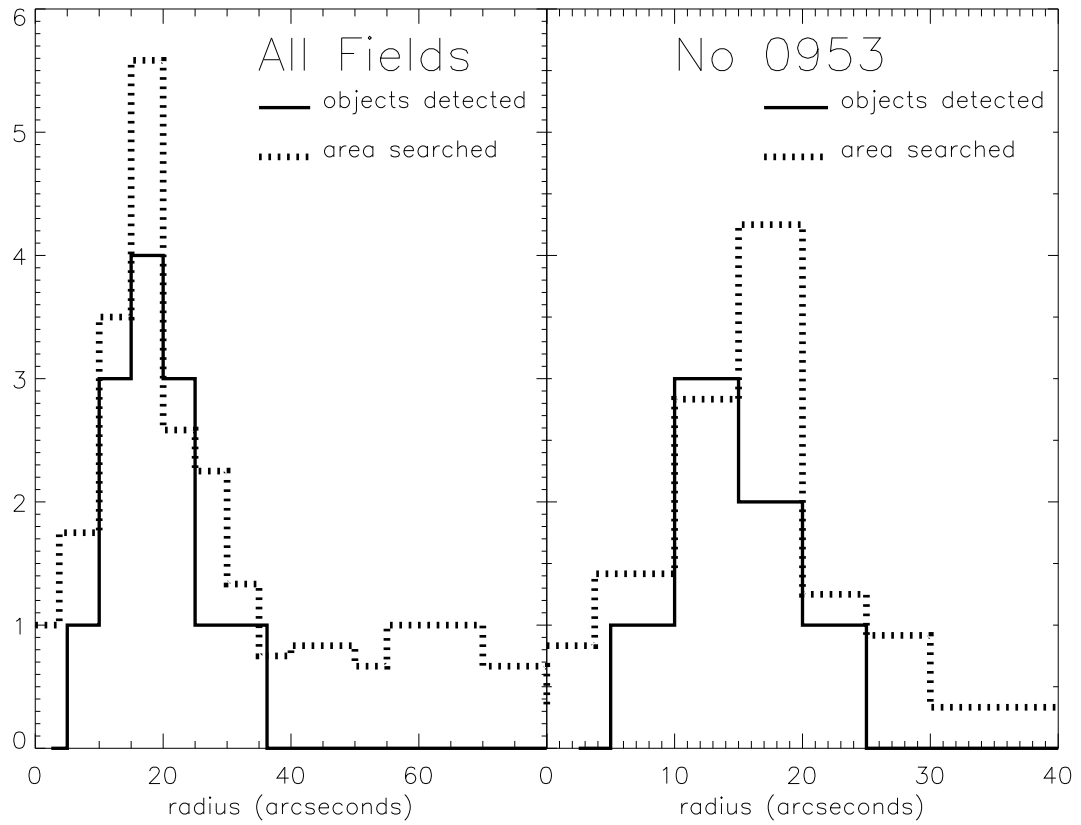


Fig. 16.— Histogram of the radial distribution of detected  $H\alpha$  emitters. The surveyed area has been normalized to the scale of the number detections and plotted, in order to show the similarity in the shape of the radial distribution of the area surveyed and the detections.

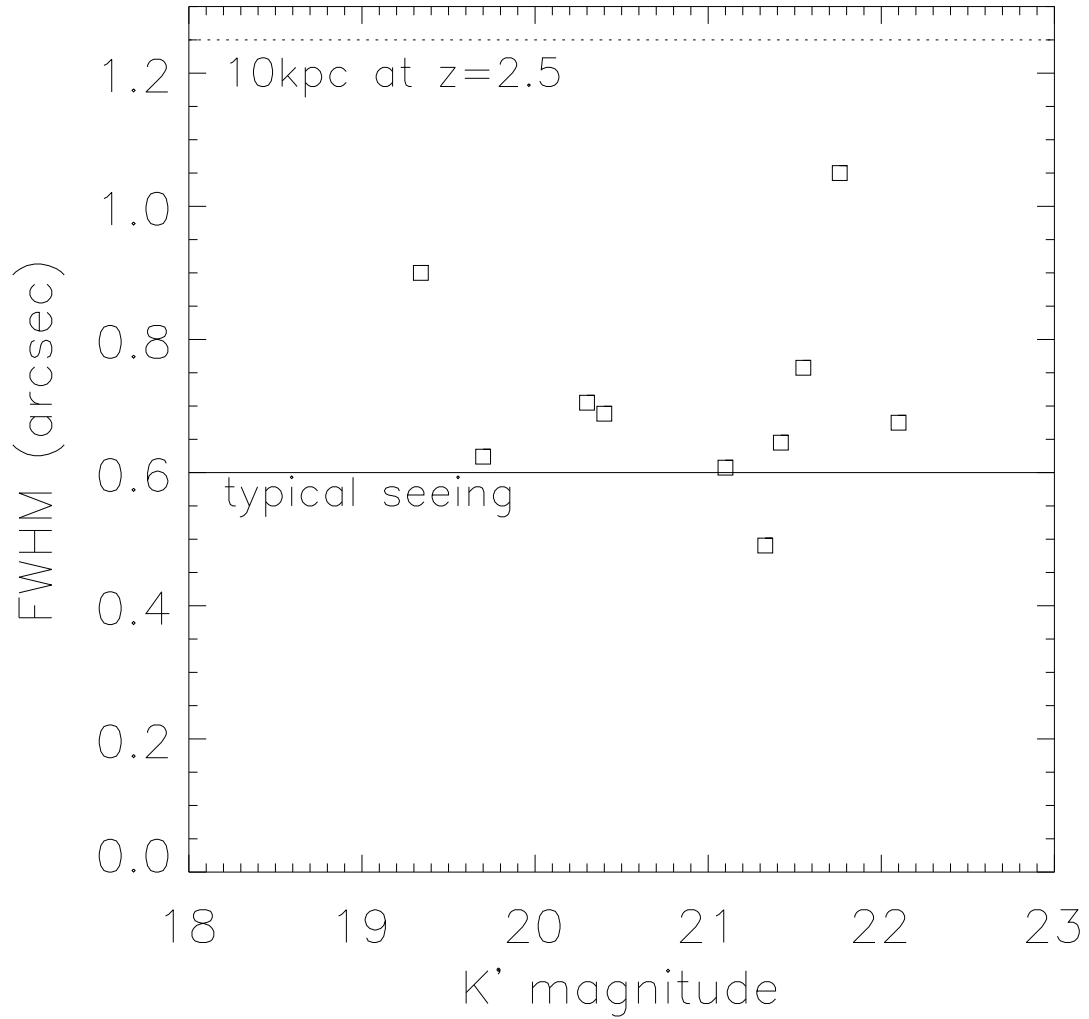


Fig. 17.— FWHM of H $\alpha$  emitters vs. K' magnitude. The solid line indicates the typical (0.6'') seeing, and the dotted line indicated 10kpc at  $z=2.5$ , for  $H_0 = 50$ ,  $q_0 = 0.5$ . The object below the typical seeing line is 0953+549D and was observed in usually good (0.35'') seeing.